Supporting Information

Record-Setting Sorbents for Reversible Water Uptake by Systematic Anion-Exchanges in Metal-Organic Frameworks

Adam J. Rieth[1], Ashley M. Wright[1], Grigorii Skorupskii[1], Jenna L. Mancuso[2], Christopher H. Hendon[2], and Mircea Dincă[1]*

[1]Department of Chemistry, Massachusetts Institute of Technology, 77 Mass. Ave. Cambridge, Massachusetts, 02139, United States.

[2] Materials Science Institute, Department of Chemistry and Biochemistry, University of Oregon, Eugene, Oregon, 97403, United States

*Corresponding Author: mdinca@mit.edu

Table of Contents **Pages**

Section S1. General Information.

Materials and Methods

$NiCl_2 \cdot 6H_2O$ (Strem Chemicals), HCl (32-35%, BDH – VWR Analytic) methanol (99.9%, VWR), *N*,*N*-dimethylformamide (99.8%, Millipore), 1-chloro-2,4-dinitrobenzene (99%, TCI), Catechol (99%, Sigma-Aldrich), K_2CO_3 (99%, Sigma-Aldrich), Sn Powder (150 micron, 99.5%, Sigma-Aldrich), diethyl ether (99%, Sigma-Aldrich), Trimethylsilyl bromide (97%, Sigma-Aldrich), Acetone (ACS grade, Macron Chemical), Fuming HNO_3 (90% min, Macron), H_2SO_4 (95-98%, BDH Chemicals), Acetic Acid (ACS grade, VWR BDH Chemicals), $NaNO_2$ (98%, Alfa Aesar), Ethanol (200 proof, Koptec), KOH (ACS grade, BDH chemicals), CsF (99%, Beantown Chemicals) were used as received. Benzene (ACS grade, EMD) was purged with argon, and subjected to three freeze-pump-thaw cycles before bringing into a nitrogen-filled glovebox and stored over 3 Å molecular sieves.

Powder X-ray diffraction (PXRD) patterns were recorded with a Bruker D8 Advance II diffractometer equipped with a θ/2θ Bragg-Brentano geometry and Ni-filtered CuKα radiation ($K\alpha_1$ = 1.5406 Å, $K\alpha_2$ = 1.5444 Å, $K\alpha_2$/ $K\alpha_1$ = 0.5). The tube voltage and current were 40 kV and 40 mA, respectively. Samples for PXRD were prepared by placing a thin layer of the appropriate material on a zero-background silicon crystal plate.

Nitrogen adsorption isotherms were measured by a volumetric method using a Micromeritics ASAP 2020 gas sorption analyzer. A typical sample of ca. 40 mg of metal-organic framework, pre-activated at 100°C to remove all residual solvent, was transferred in an Ar filled glovebox to a pre-weighed analysis tube. The tube with sample inside was weighed again to determine the mass of the sample. The tube was capped with a Micromeritics TranSeal, brought out of the glovebox, and transferred to the analysis port of the gas sorption analyzer. Free space correction measurements were performed using ultra-high purity He gas (UHP grade 5, 99.999% pure). Nitrogen isotherms were measured using UHP grade nitrogen. All nitrogen analyses were performed using a liquid nitrogen bath at 77 K. Oil-free vacuum pumps were used to prevent contamination of sample or feed gases.

Water vapor adsorption and desorption isotherms were measured by a volumetric method using a Micromeritics ASAP 2020 gas sorption analyzer with a vapor dose option and a heated manifold. A typical sample of ca. 40 mg of metal-organic framework, pre-activated at 100°C to remove all residual solvent, was transferred in an Ar filled glovebox to a pre-weighed analysis tube. The tube with sample inside was weighed again to determine the mass of the sample. The tube was capped with a Micromeritics TranSeal, brought out of the glovebox, and transferred to the analysis port of the gas sorption analyzer. Free space correction measurements were performed using ultra-high purity He gas (UHP grade 5, 99.999% pure). Water vapor adsorption isotherms were measured using Milli-Q water. The water was degassed on the ASAP 2020 manifold prior to measurement. All water analyses were performed using water baths held at constant temperature with a recirculating chiller. The manifold was held 10 °C above the temperature of the sample water bath, and the vapor dosing tube was held 15 °C above the temperature of the sample water bath. Oil-free vacuum pumps were used to prevent contamination of sample or feed gases.

Variable-temperature water vapor adsorption isotherms as well as all water cycling experiments were measured by a gravimetric method using a Hiden Analytical XEMIS microbalance with a vapor dose option and a heated manifold. A typical sample of ca. 5 mg of metal-organic framework, pre-activated at 100°C to remove all residual solvent, but later exposed to air, was loaded into the microbalance basket. All water analyses were performed using a programmable water bath with a recirculating chiller. Oil-free vacuum pumps were used to prevent contamination of sample or feed gases.

Diffuse reflectance infrared Fourier transform spectroscopy (DRIFTS) measurements were performed using a Bruker Tensor 37 IR spectrometer equipped with a liquid nitrogen cooled mercury cadmium telluride detector and a Pike DiffusIR accessory. A sample of Co_2Cl_2BTDD, pre-activated at 150 °C under vacuum to remove all water, was diluted with KBr in a ratio of approximately 1:5 (MOF:KBr) in an argon-filled glovebox. The resulting solid solution was then packed into a ceramic cup and sealed in the DiffusIR cell. The cell was brought out of the box, and a static dry spectrum was recorded with the cell sealed. Two gas streams of flowing argon (UHP grade 5.0, Airgas), one wet (bubbled through a fine frit through MilliQ H_2O) and one dry, were each flow controlled using mass flow controllers (MFCs), and joined together at a T fitting before connecting to the DRIFTS cell. The wet stream and dry stream were controlled via the mass flow controllers (MFCs) to change relative humidity (RH) every 20 minutes (a time period previously demonstrated to result in saturation of the IR spectrum at all loadings). The MFCs were controlled such that the total flow rate was constant at 1 liter per minute (LPM) (e.g. for 40% RH, 0.4 LPM wet, 0.6 LPM dry). The temperature for all measurements was 20 °C. Spectra were recorded at the end of the period at which the sample atmosphere was at each RH, every 20 minutes. Data was transformed using the Kubelka-Munk function.[1]

Energy dispersive X-ray spectroscopy (EDS) analyses were conducted using a FEI Tecnai Multipurpose Digital TEM, using the EDAX system (Windowless detector) with Team software, operated with an acceleration voltage of 100 keV. Samples were drop-cast onto Cu TEM grids from powder dispersed in methanol.

X-ray photoelectron spectroscopy (XPS) was performed at the Harvard Center for NanoscaleSystems (Cambridge, MA, USA) on a Thermo Scientific K-Alpha system equipped with an Al source and 180° double focusing hemispherical analyzer and 128-channel detector using a 400 μm X-ray spot size.

NMR Spectroscopy was performed in the Massachusetts Institute of Technology (MIT) Department of Chemistry Instrumentation Facility (DCIF) using a Bruker AVANCE NEO 400 MHz spectrometer equipped with a broadband probe.

High-resolution synchrotron powder X-ray spectroscopy was performed using the mail-in program at beamline 11-BM at the Argonne National Laboratory (ANL) Advanced Photon Source (APS). Samples were packed into a Kapton capillary and the ends were sealed using epoxy. Samples were mounted into Kapton capillary sample holders provided by the beamline and shipped to the beamline. Powder patterns were collected with the standard automated experimental setup[2–4] at 100 K using 0.412805 Å X-rays.

Thermogravimetric analysis (TGA) was performed on a TA Instruments Q500 Thermogravimetric Analyzer at a heating rate of 1 °C/min under a nitrogen gas flow of 90 mL/min.

Elemental Analyses were performed by Robertson Microlit Laboratories, Ledgewood NJ.

	% C	% H	% N
Ni_2Cl_2BTDD			
Calc. (Dry)	31.85	0.89	18.57
Calc. (2.38 H_2O)	29.08	1.79	16.96
Found	29.45	2.52	16.74
Ni_2F_2BTDD			
Calc. (Dry)	34.35	0.96	20.03
Calc. (2.26 H_2O)	31.31	1.87	18.26
Found	32.10	2.72	17.34
Ni_2Br_2BTDD			
Calc. (Dry)	26.62	0.74	15.52
Calc. (2.61 H_2O)	24.49	1.58	14.28
Found	24.88	1.77	13.74
$Ni_2(OH)_2BTDD$			
Calc. Dry	34.68	1.46	20.22
Calc. (2.13 H_2O)	31.73	2.28	18.51
Found	32.59	2.76	17.28

Computational Methods

All structures were fully optimized within the DFT construct using PBEsol[5] as implemented in Vienna *Ab-Initio* Software Package (VASP)[6] with a projector-augmented-wave plane wave basis set. A 500 eV plane-wave cutoff was employed with a 2 x 2 x 2 k-grid. Calculations were performed with spin polarization and Ni atoms were initiated as, and optimized to, the high-spin state.

Calculation of the Characteristic Curve

In order to make the loading dependent on only one free variable ("energy") rather than two (P,T), we constructed a characteristic curve.[7–9] The energy parameter used is the adsorption potential (A), which is the Gibbs free energy of adsorption with inverse sign:

$$A = RT \ln\left(\frac{p_o(T)}{p}\right)$$

p_o is the saturation vapor pressure of the working fluid at the temperature of analysis, p is the pressure at each loading value, R is the ideal gas constant, and T is the analysis temperature.

Isotherms measured at different temperatures should collapse onto a single characteristic curve. Water isotherms for **Ni_2Cl_2BTDD** and **Ni_2Br_2BTDD** were measured at 283 K, 293 K, and 298 K. After calculating the characteristic curve using each of these isotherms, it is evident that they all collapse into a single characteristic curve confirming the validity of the characteristic curve model.

Calculation of the Enthalpy of Adsorption

The Clausius-Clayperon equation was used to determine the enthalpy of adsorption (ΔH_{ads}). Loadings at two different temperatures were calculated from the characteristic curve, and these values were then used to calculate the heat of adsorption according to the integrated Clausius-Clayperon equation:

$$\ln\frac{P_1}{P_2} = -\frac{\Delta H_{ads}}{R}\left(\frac{1}{T_1} - \frac{1}{T_2}\right)$$

Section S2. Synthetic Methods.

Improved Synthetic Pathway to the Ligand H_2BTDD

Literature methods for the synthesis of H_2BTDD normally begin with the relatively expensive dibenzodioxin core.[10] We synthesized the ligand using more scalable methods beginning with 1-chloro-2,4-dinitrobenzene (**1**) according to the following scheme:

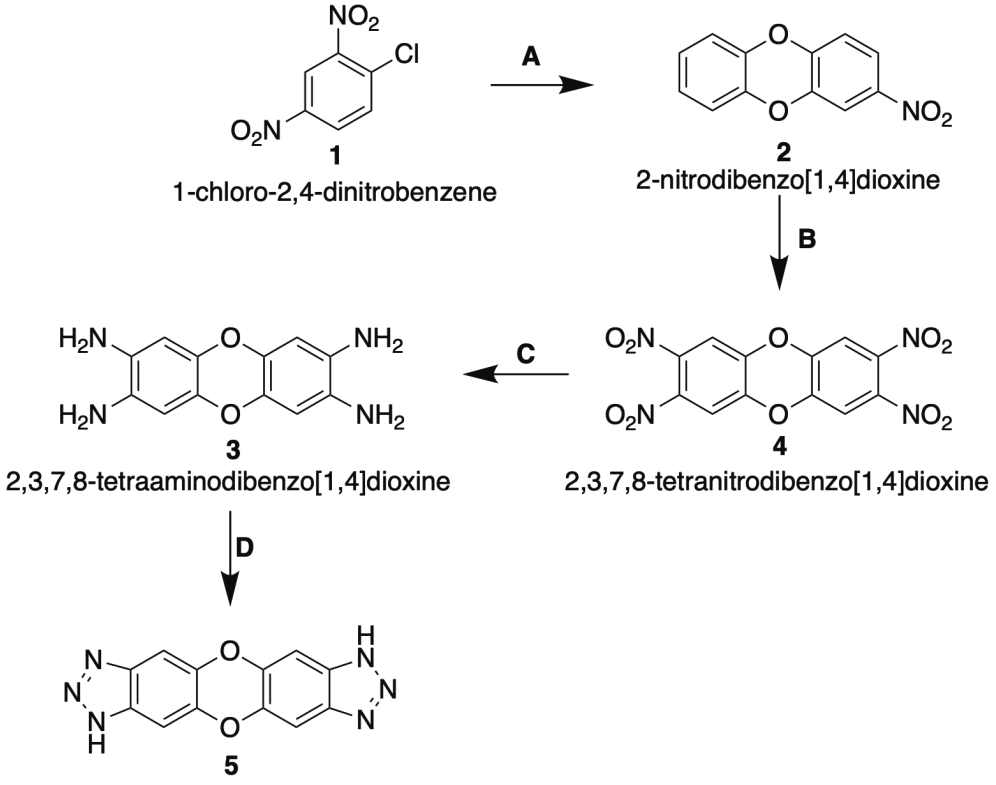

Scheme 1: Novel synthesis pathway to H_2BTDD, compound **5**.

Reaction A. To a warm (60 °C) stirring solution of 11.9 g catechol and 30.02 g potassium carbonate in 120 mL N-N-dimethylformamide in a 250 mL round bottom flask was added 20 g 1-chloro-2,4-dinitrobenzene. The mixture was heated to reflux for 3 hours, then cooled to room temperature. The mixture was then poured into 250 mL crushed ice. The solids were separated by filtration and washed with deionized water. The yellow solids obtained were dissolved in 1000 mL hot acetone, which was cooled to RT and 400mL DI water was slowly added. The resulting precipitate was filtered, washed with deionized water, and dried to obtain 22.9 g of 2-

nitrodibenzo[1,4]dioxin (**2**). Purification can also proceed by recrystallization from a 50:50 mixture of chloroform and methanol to obtain yellow crystals.

Reaction B. In a 500mL RBF, 90 mL fuming nitric acid was added to 22.9 g 2-nitrodibenzo[1,4]dioxin. A condenser was equipped and 60 mL sulfuric acid added slowly through the top of condenser. The reaction was heated at 70 °C overnight, then cooled to room temperature. The mixture was then filtered to obtain the product, 2,3,7,8-tetranitrodibenzo[1,4]dioxin (**3**).

Reaction C. In a 500 mL 2 neck round bottom flask, 9.2 g 2,3,7,8-tetranitrodibenzo[1,4]dioxin was added to 190 mL hydrochloric acid and a stir bar. A condenser was equipped. 48 g powdered Sn was added in small portions while stirring, slowly to minimize foaming of the reaction mixture. After all Sn was added and the off-gassing had subsided, the mixture was heated to reflux in an oil bath overnight. Then, the mixture was cooled to room temperature, then cooled in an ice bath, filtered, and washed with concentrated hydrochloric acid, ethanol, then diethyl ether. The obtained solids, the tetra-hydrochloric acid salt of 2,3,7,8-tetraaminodibenzo[1,4]dioxin (**4**), were dried under vacuum.

Reaction D. *Normally performed directly after isolation of product from D.* To a suspension of 6.4 g of the tetra-hydrochloric acid salt of 2,3,7,8-tetraaminodibenzo[1,4]dioxin, 60 mL acetic acid, and 20 mL deionized water in a 250 mL round bottom flask on a salted ice bath was added a solution of 2.75 g $NaNO_2$ and water (20 mL) over ten minutes. Note that before addition of the oxidant, the reaction is a white, free-flowing suspension and that over the addition (which was carried out drop wise) the reaction changes color from green to orange to brown. After addition was complete, the reaction was allowed to stir an additional 30 minutes at this temperature, then diluted with 50 mL H_2O. The product was filtered, washed with water, ethanol, and diethyl ether. Tan solids were obtained that were the product, bis(1H-1,2,3-triazolo[4,5-b],[4′,5′-i])dibenzo[1,4]dioxin), or H_2BTDD (**5**).

Synthesis of Ni_2X_2BTDD MOFs.

The synthesis of Ni_2Cl_2BTDD broadly followed methods in the literature[11] with increased acid concentration and temperature. In a typical synthesis, 200 mg H_2BTDD (0.75 mmol) was dissolved in 200 mL N,N'-dimethylformamide (DMF) in a 500 mL jar by stirring and heating to approximately 100°C. The clear solution was then cooled to room temperature. In a separate 500 mL jar, 1.65 mmol (2.2 eq.) nickel chloride hydrate was dissolved in a solution of 200 mL methanol and 128 mL concentrated hydrochloric acid. The clear solutions were combined, capped, and heated to 100°C in an oven for 2 days. After this time, the reaction mixture was removed from the oven and filtered to collect the solids. The solids were washed with DMF and methanol. Solvent exchange of DMF was carried out by Soxhlet extraction with methanol for approximately 48 hours. The materials were then activated under dynamic vacuum at 150°C for 24 hours.

The synthesis of $Ni_2(OH)_2$BTDD followed the methods for the synthesis of $Co_2(OH)_2$BTDD and the smaller pore $Co_2(OH)_2$BBTA reported in the literature.[12] Briefly, beginning with the as-synthesized Ni_2Cl_2BTDD material, 10 eq. of KOH per Cl^- were dissolved in deionized water and added to a suspension of MOF in deionized water to form a 0.05 M hydroxide solution. The

suspension was stirred overnight, then filtered, the solids were washed with DMF and methanol, and then activated at 100°C under dynamic vacuum.

To synthesize Ni_2F_2BTDD, 0.751 mmol as-synthesized Ni_2Cl_2BTDD material was suspended in 80 mL DMF. 5.7 g CsF (25 eq. per Cl^-) was added to the suspension, and it was stirred for 12 hours at room temperature. The suspension was then filtered on a frit and washed with 10 × 20 mL DMF and 10 × 20 mL methanol. The resulting powder was activated at 100 °C under dynamic vacuum.

To synthesize Ni_2Br_2BTDD, 100 mg of activated Ni_2F_2BTDD in a nitrogen-filled glovebox was suspended in 5 mL dry, degassed benzene. 0.066 mL (1.05 eq. per F^-) trimethylsilyl bromide was added from a syringe in one portion. The vial was left overnight, then filtered on a frit and the solids were washed with benzene. The resulting powder was activated at 100 °C under dynamic vacuum.

Section S3. Powder X-ray Diffraction Data.

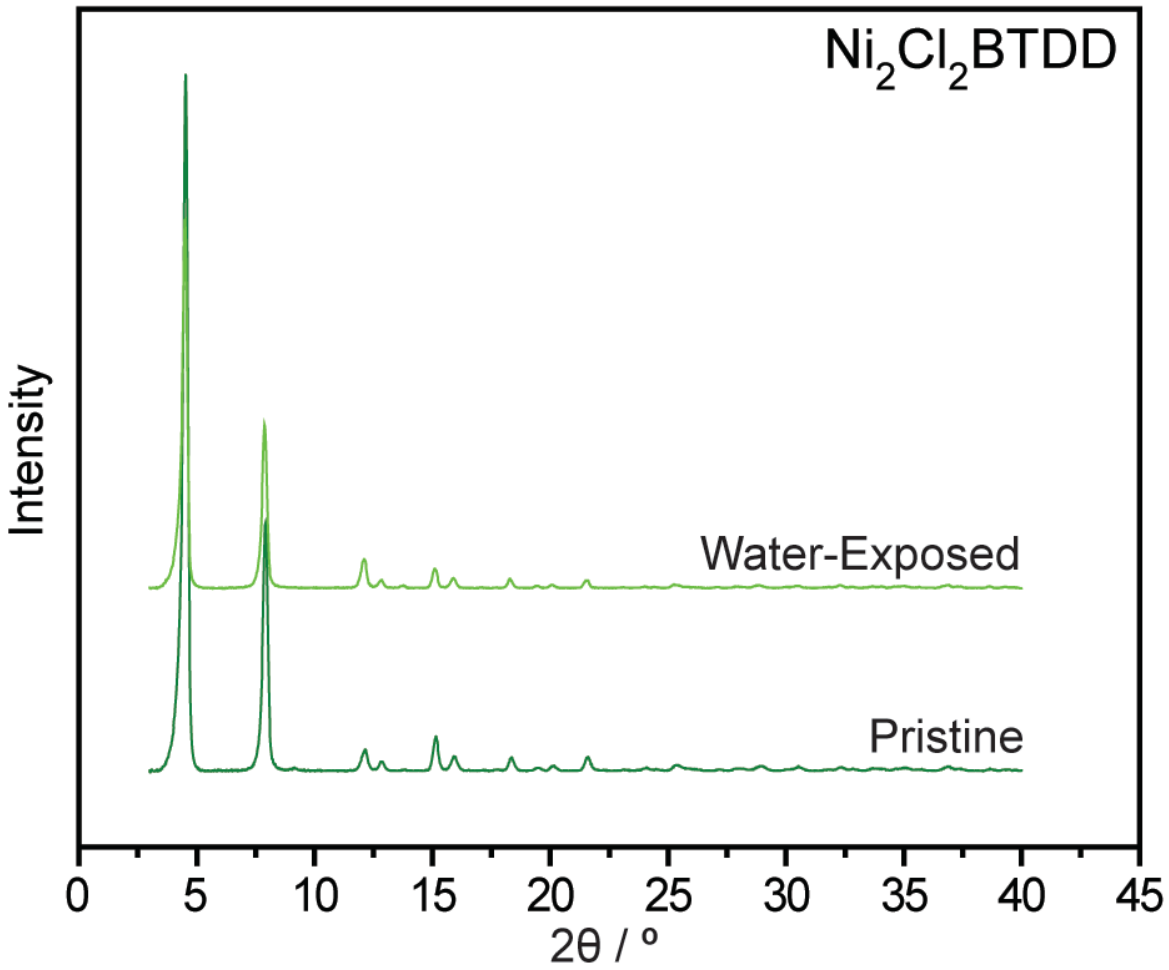

Figure S3.1. Powder X-ray diffractograms for activated samples of pristine Ni_2Cl_2BTDD (dark green), and after a single water isotherm (light green).

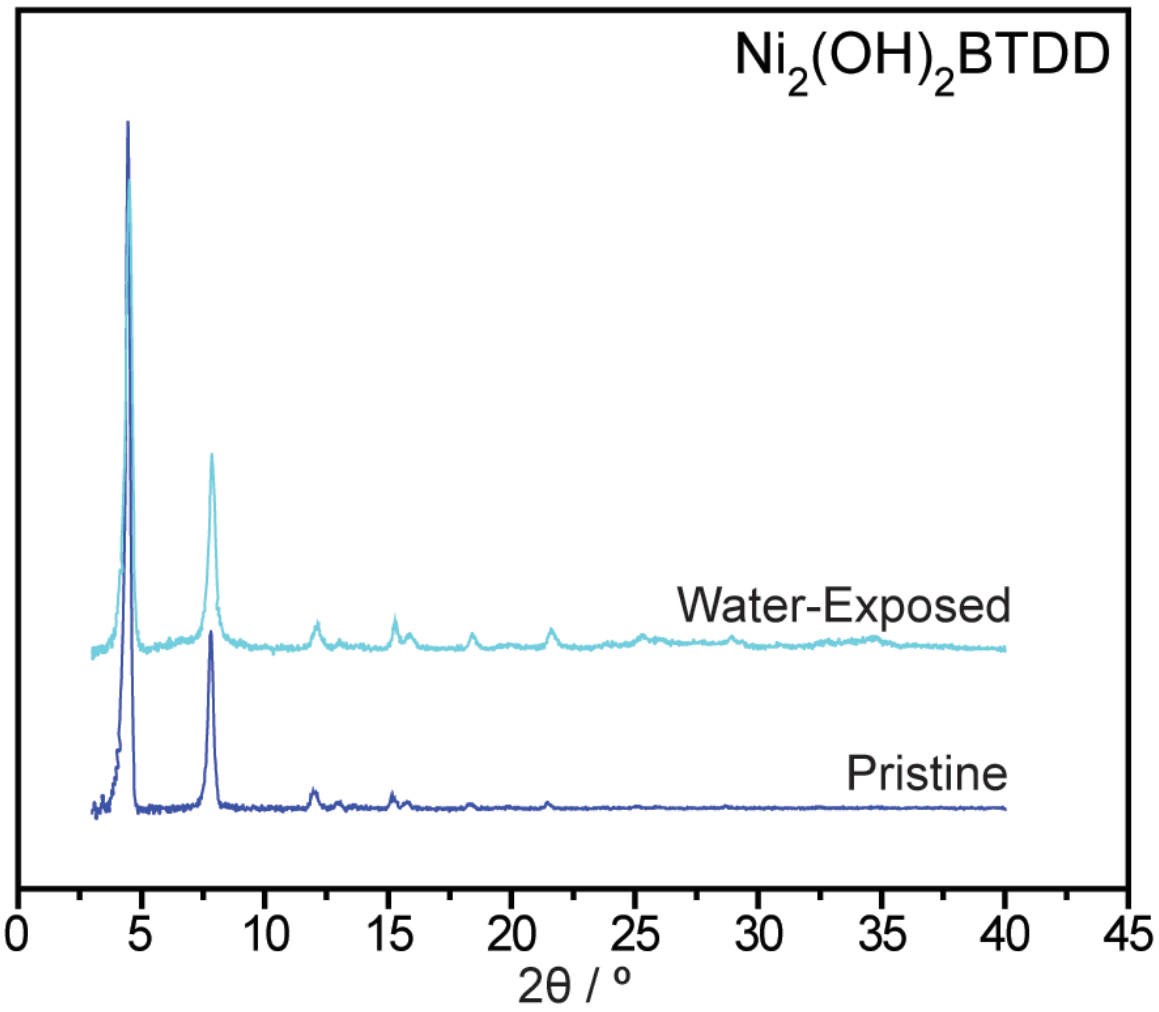

Figure S3.2. Powder X-ray diffractograms for activated samples of pristine $Ni_2(OH)_2BTDD$ (dark blue), and after a single water isotherm (light blue).

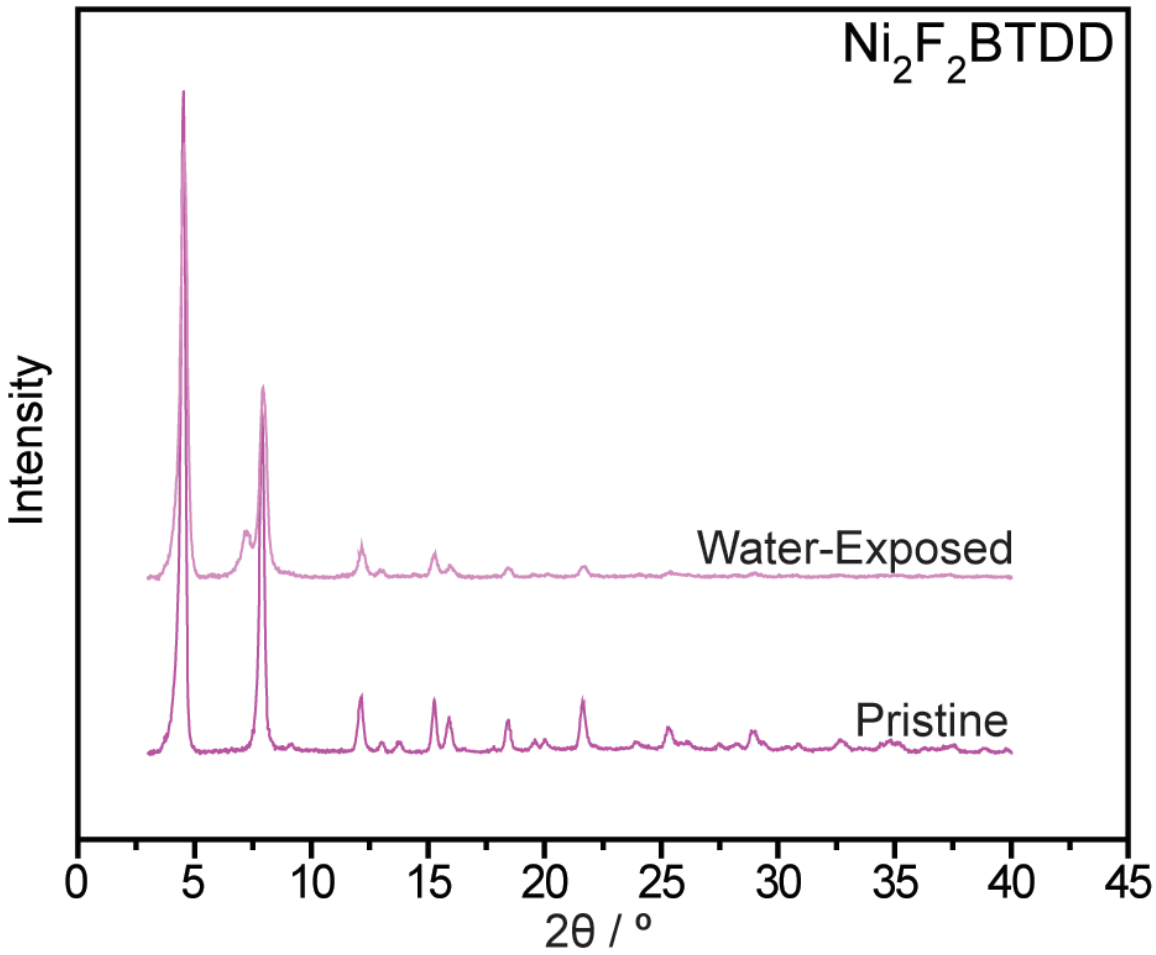

Figure S3.3. Powder X-ray diffractograms for activated samples of pristine Ni_2F_2BTDD (dark pink), and after a single water isotherm (light pink).

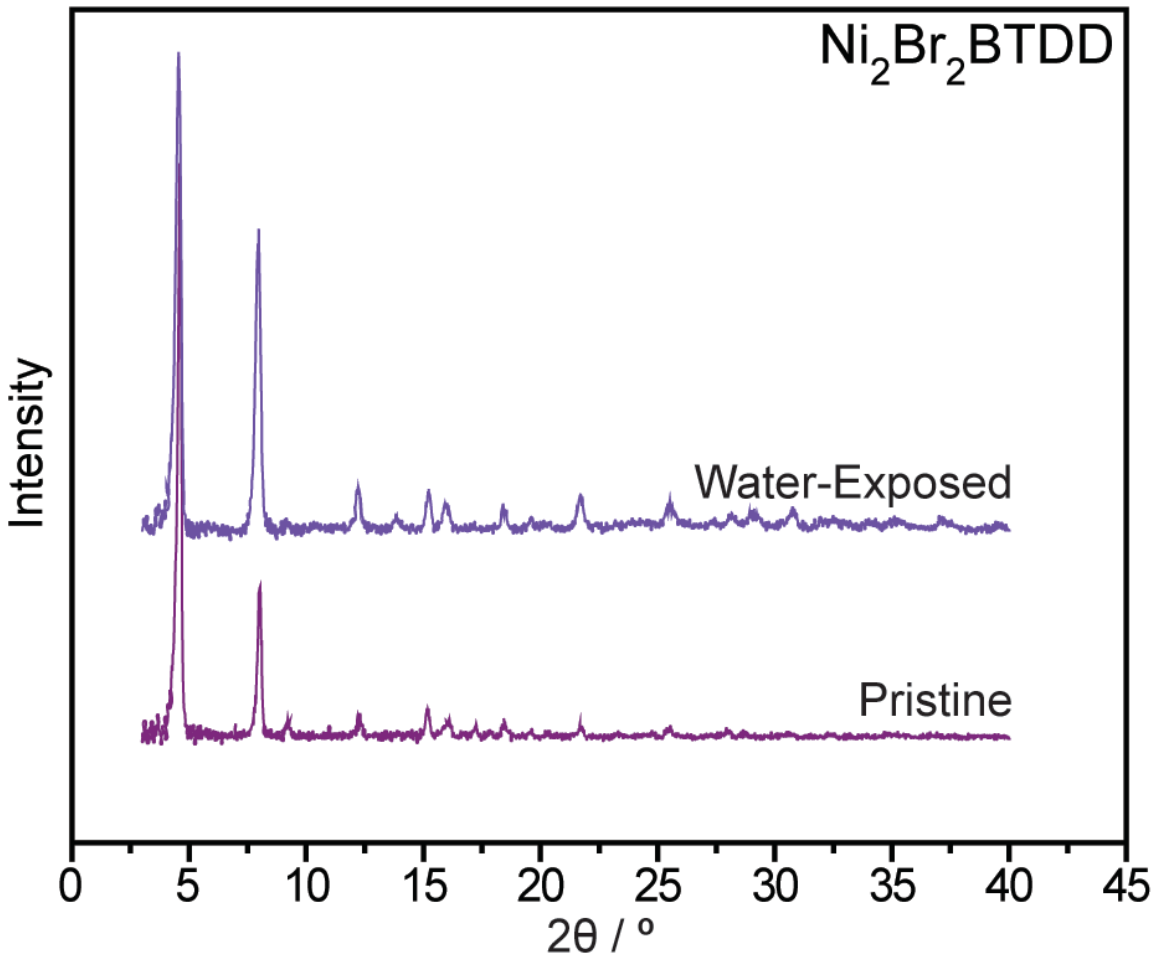

Figure S3.4. Powder X-ray diffractograms for activated samples of pristine Ni_2Br_2BTDD (dark purple), and after a single water isotherm (light purple).

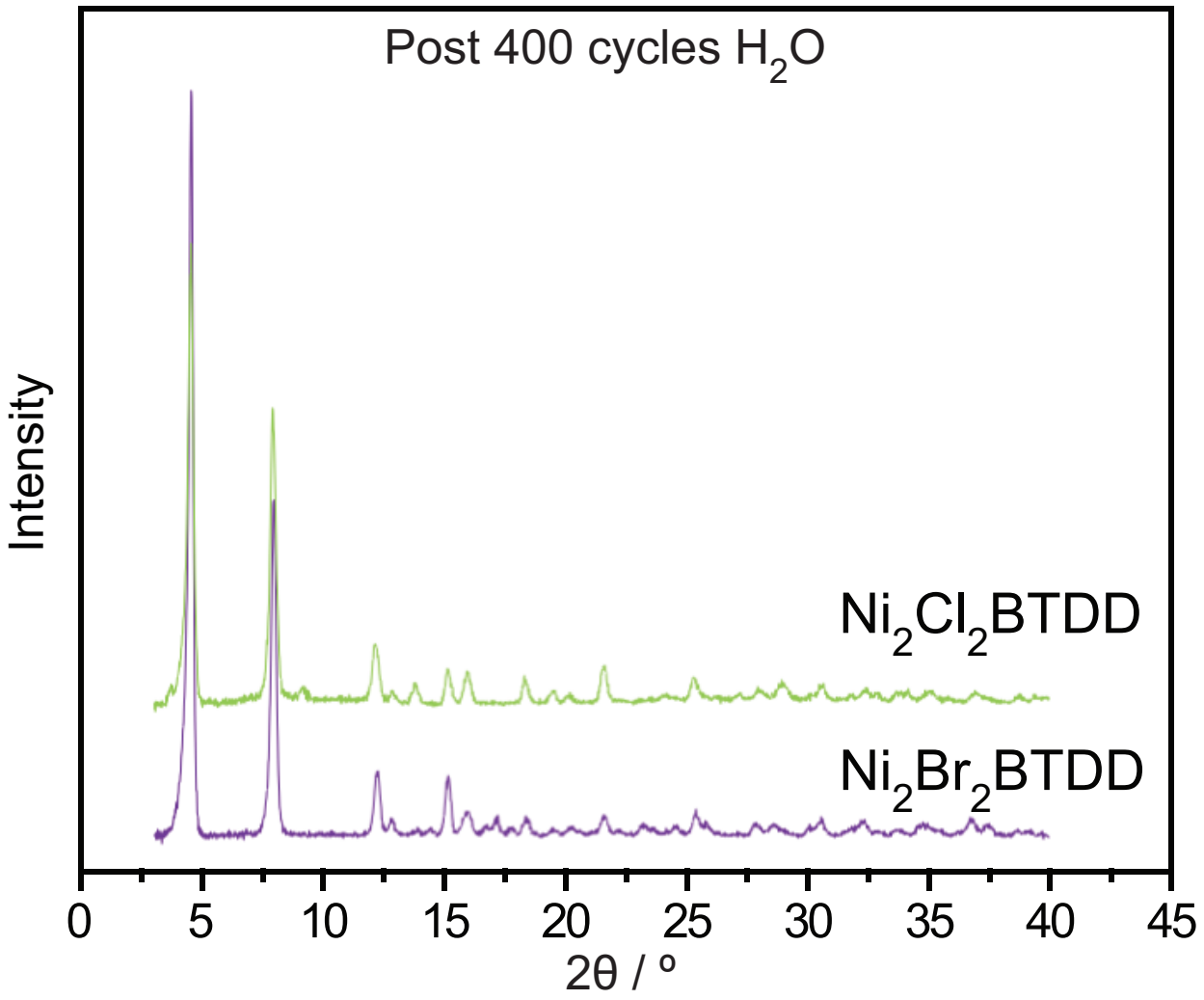

Figure S3.5. Powder X-ray diffractograms for samples after 400 cycles of water uptake and release of Ni_2Br_2BTDD (purple), and Ni_2Br_2BTDD (green).

Section S4. Nitrogen Isotherm Data.

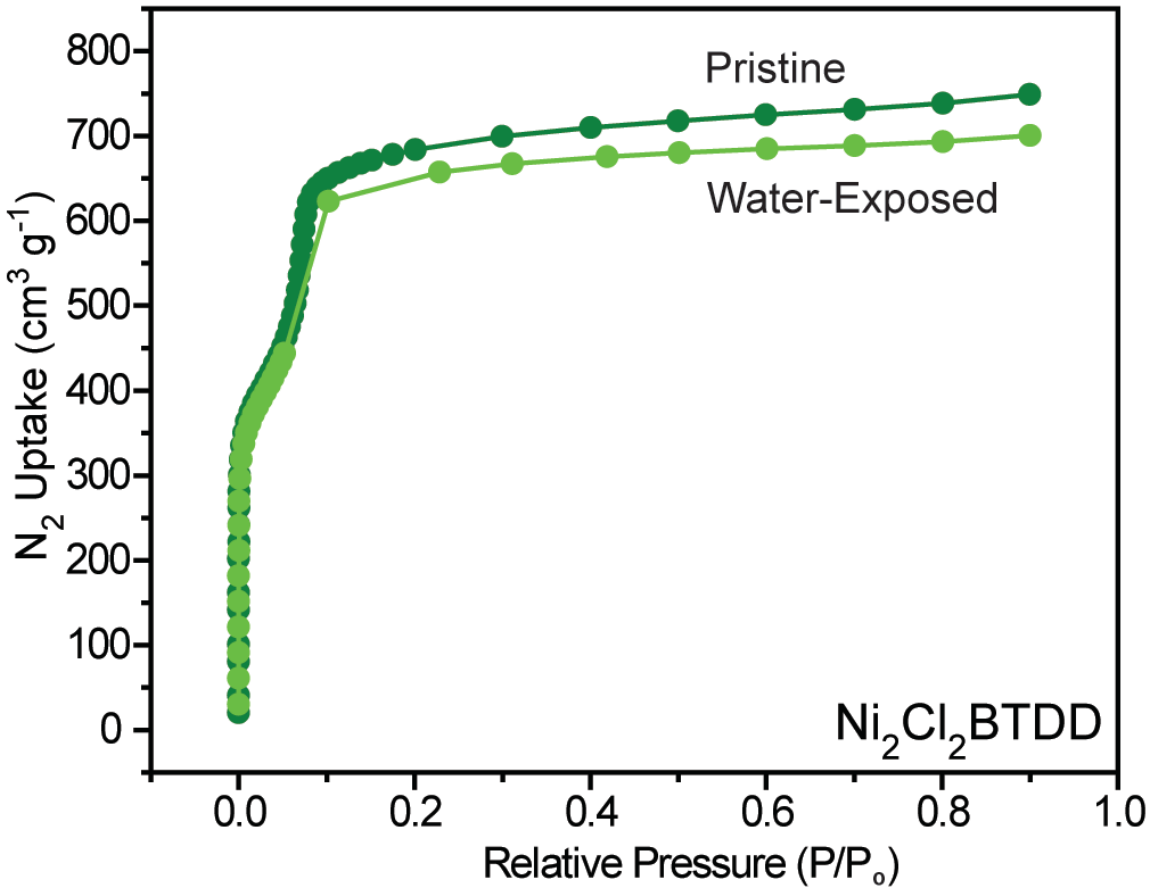

Figure S4.1. N_2 adsorption isotherms for activated samples of pristine Ni_2Cl_2BTDD (dark green), and after a single water isotherm (light green).

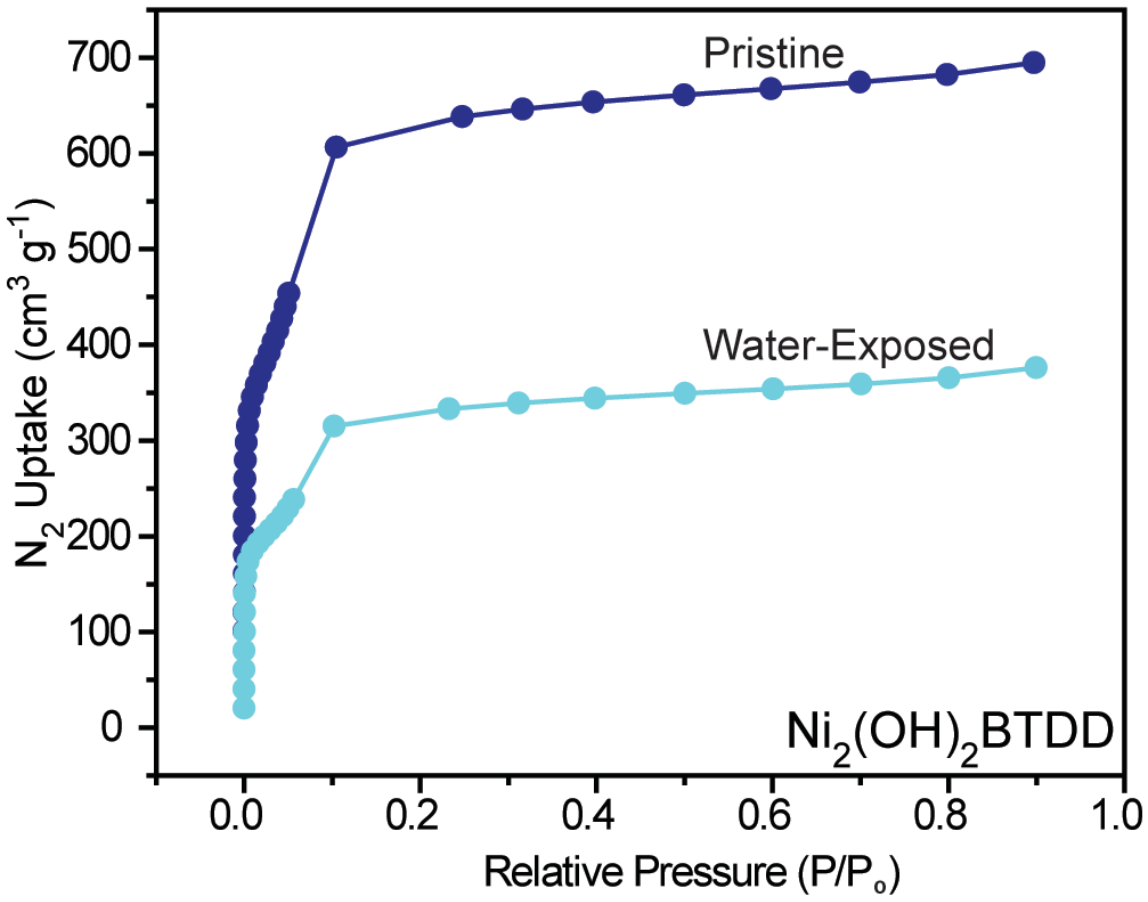

Figure S4.2. N_2 adsorption isotherms for activated samples of pristine $Ni_2(OH)_2BTDD$ (dark blue), and after a single water isotherm (light blue).

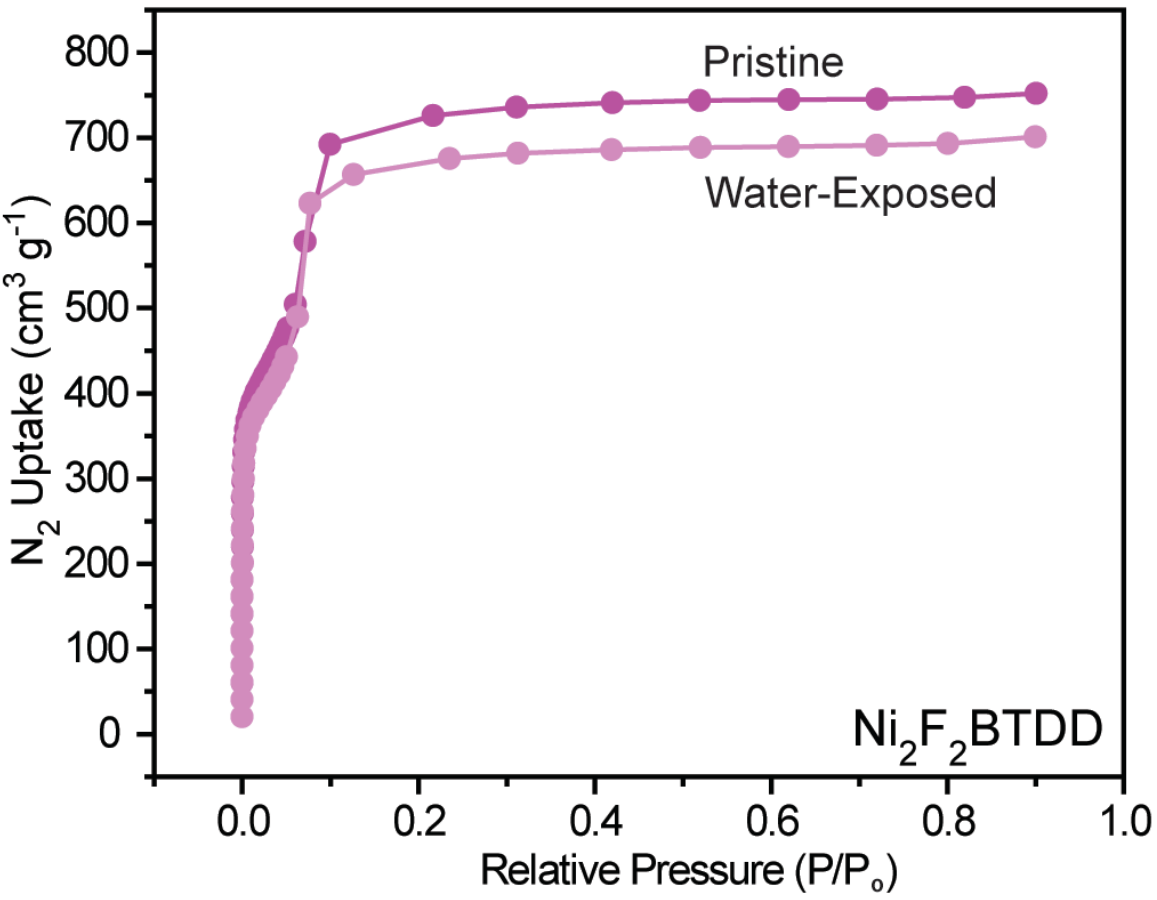

Figure S4.3. N_2 adsorption isotherms for activated samples of pristine Ni_2F_2BTDD (dark pink), and after a single water isotherm (light pink).

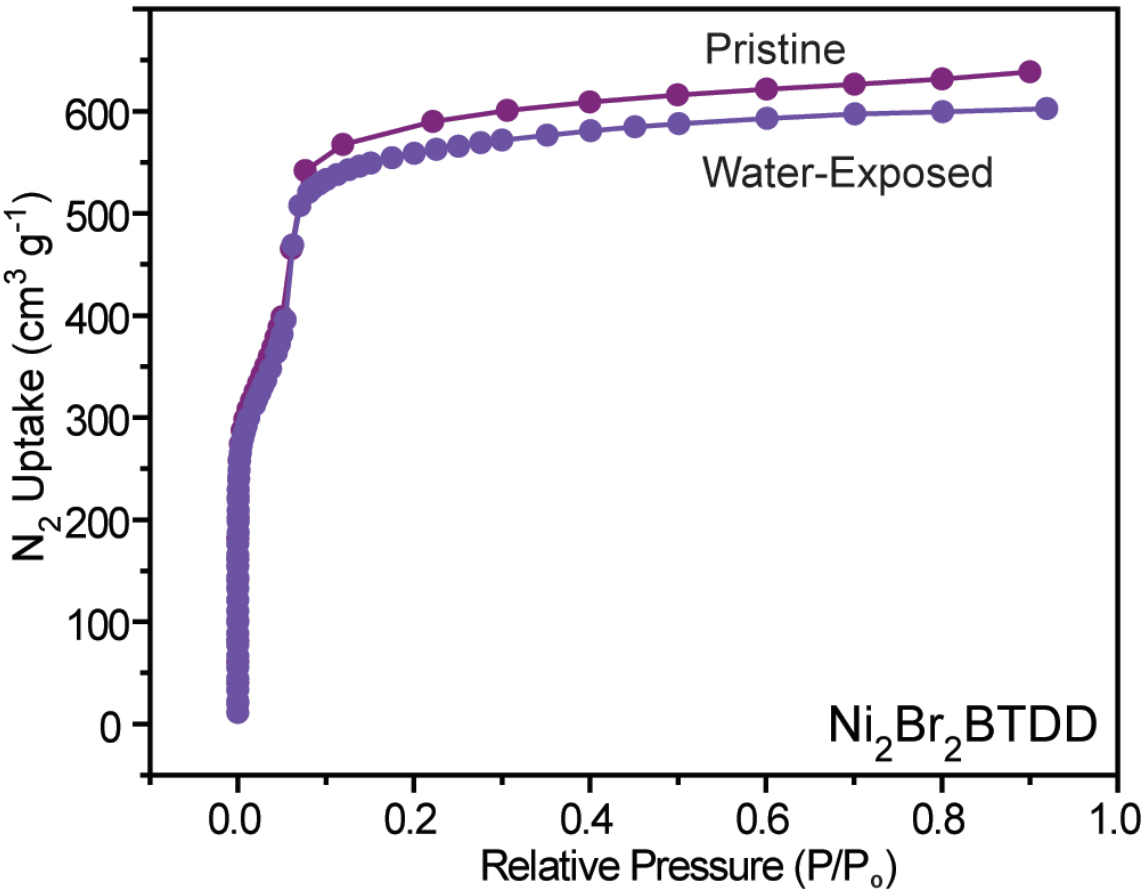

Figure S4.4. N_2 adsorption isotherms for activated samples of pristine Ni_2Br_2BTDD (dark purple), and after a single water isotherm (light purple).

Section S5. X-ray Photoelectron Spectroscopy Data.

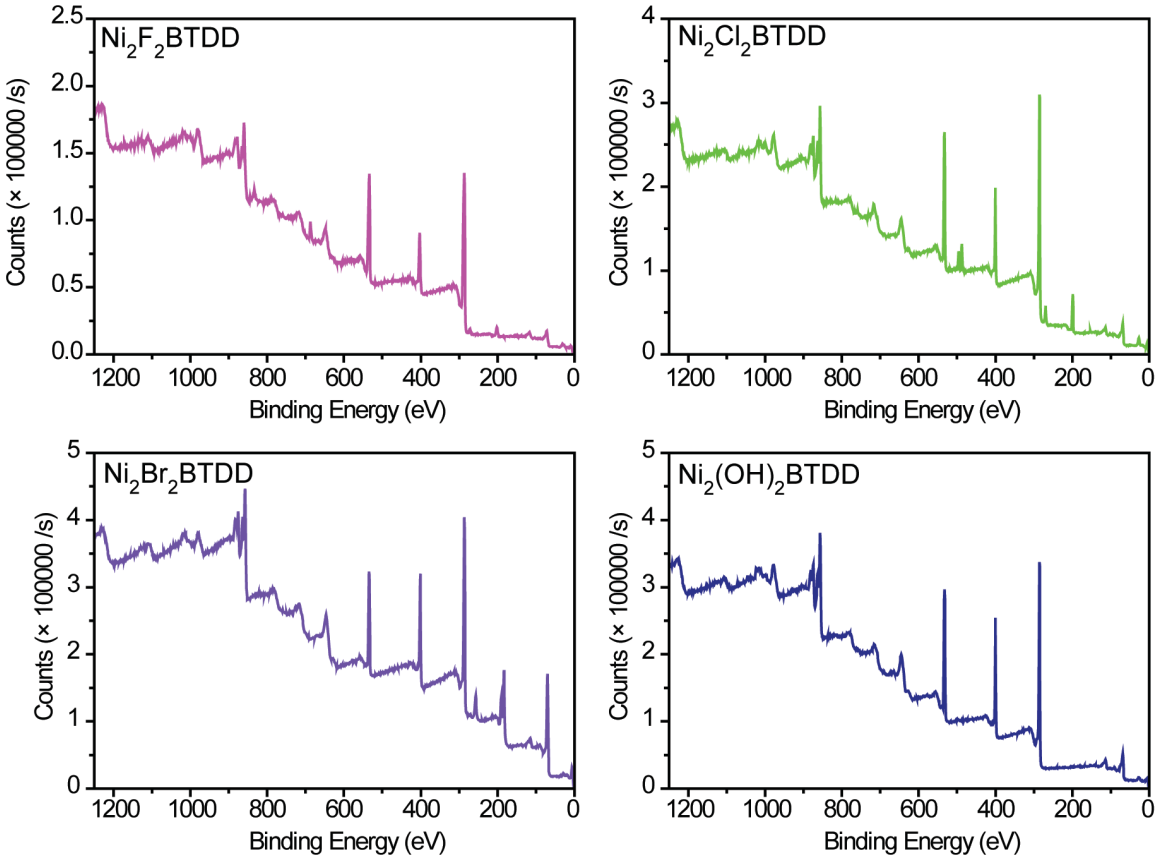

Figure S5.1: Survey X-ray photoelectron spectroscopy (XPS) for Ni_2F_2BTDD (pink), Ni_2Cl_2BTDD (green), Ni_2Br_2BTDD (purple), and $Ni_2(OH)_2BTDD$ (navy).

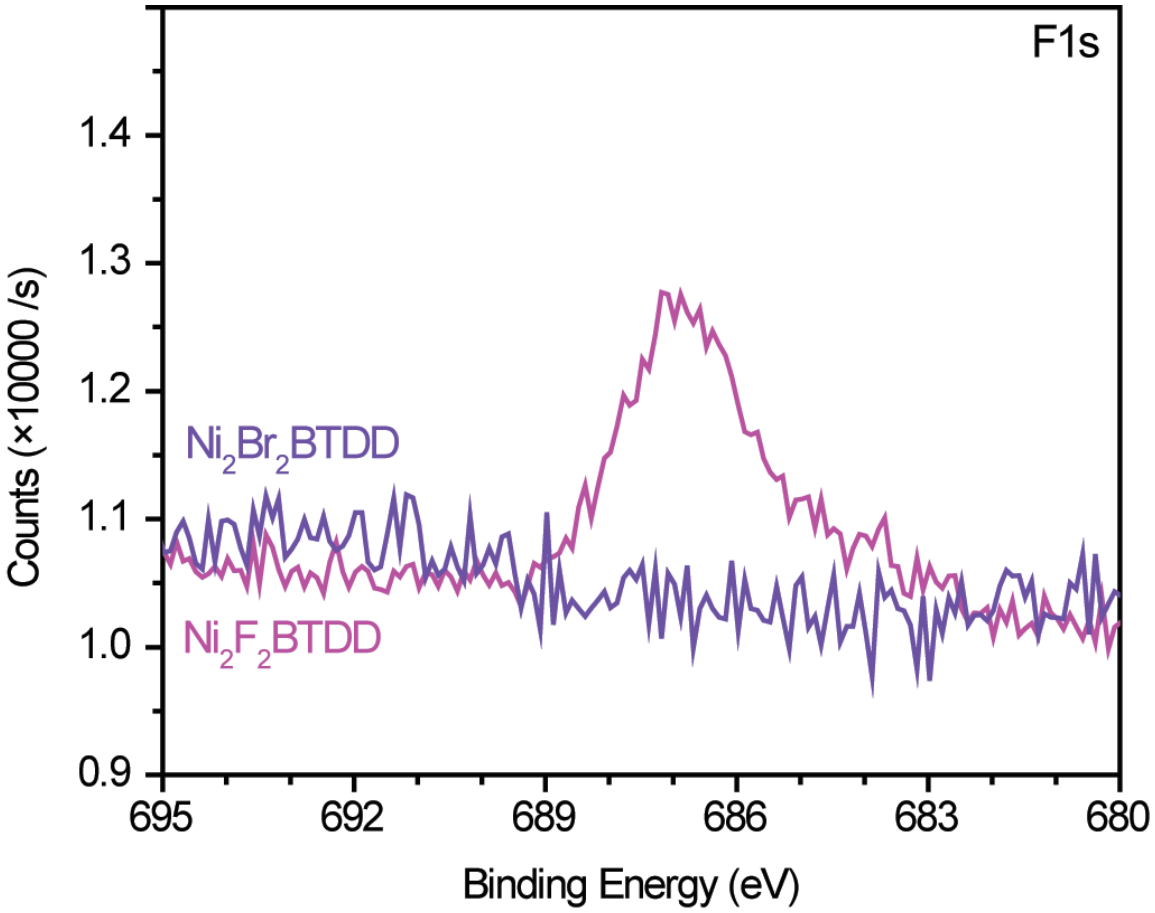

Figure S5.2: Fluoride F1s energy X-ray photoelectron spectroscopy (XPS) for Ni_2F_2BTDD (pink) and Ni_2Br_2BTDD (purple).

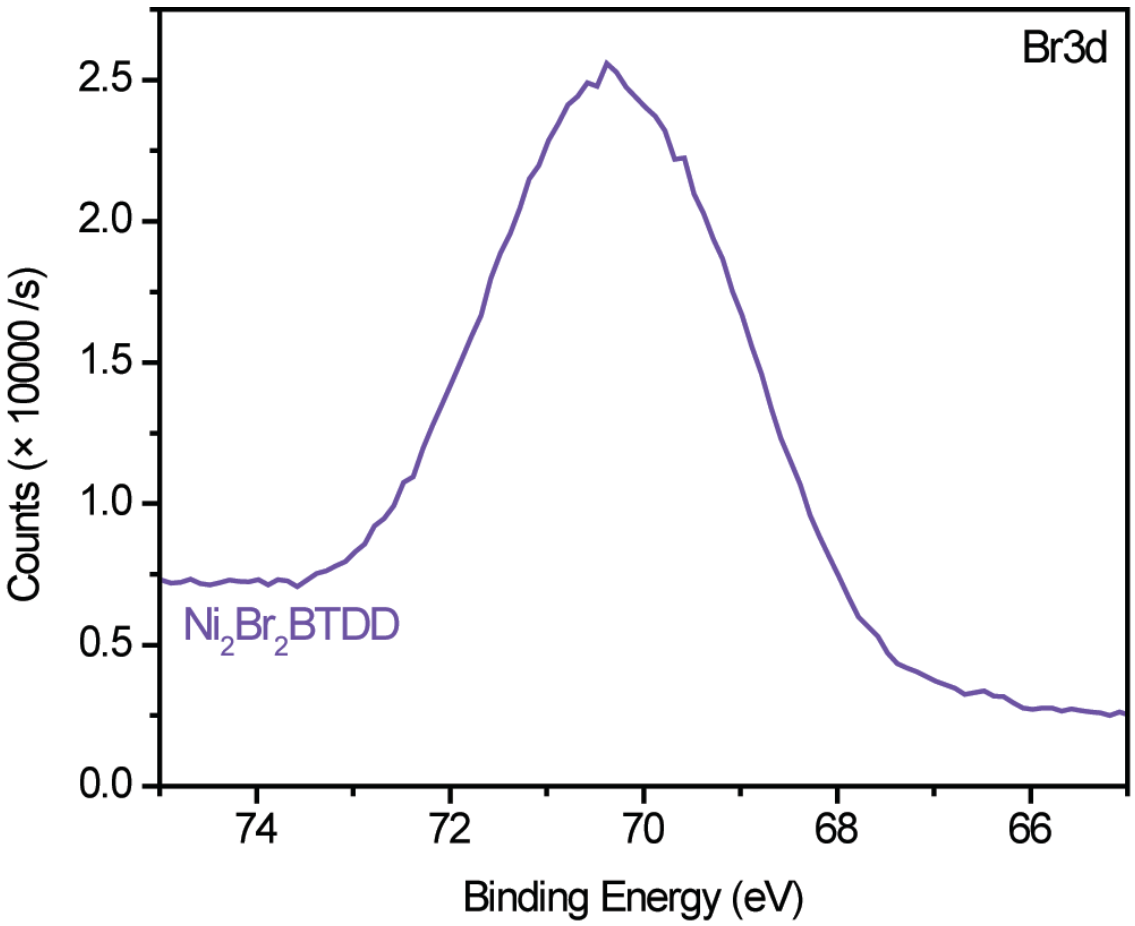

Figure S5.3: Bromide Br3d energy X-ray photoelectron spectroscopy (XPS) for Ni_2Br_2BTDD (purple).

Section S6. Infrared Spectroscopy Data.

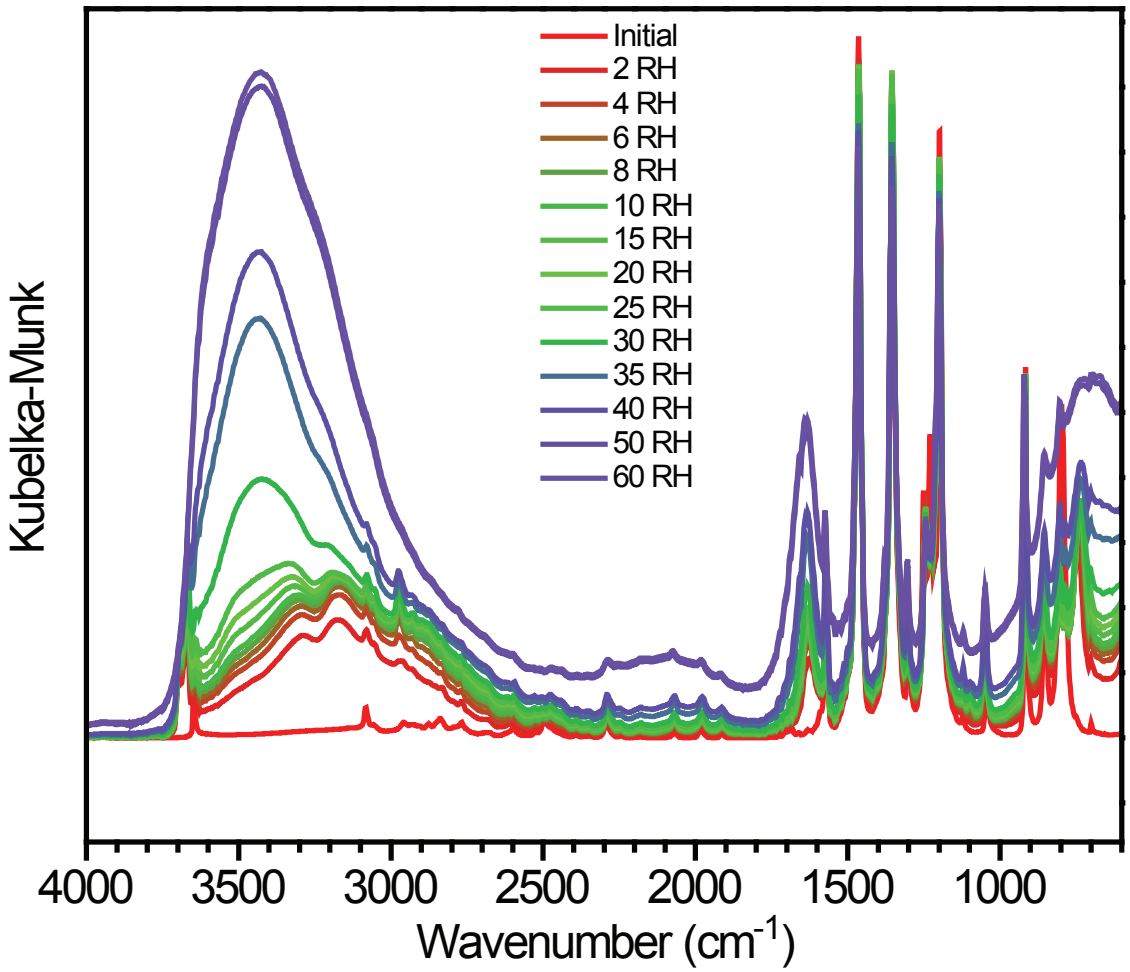

Figure S6.1. Diffuse-Reflectance Infrared Spectroscopy (DRIFTS) of the water adsorption process in $Ni_2(OH)_2BTDD$ under controlled relative humidity (RH).

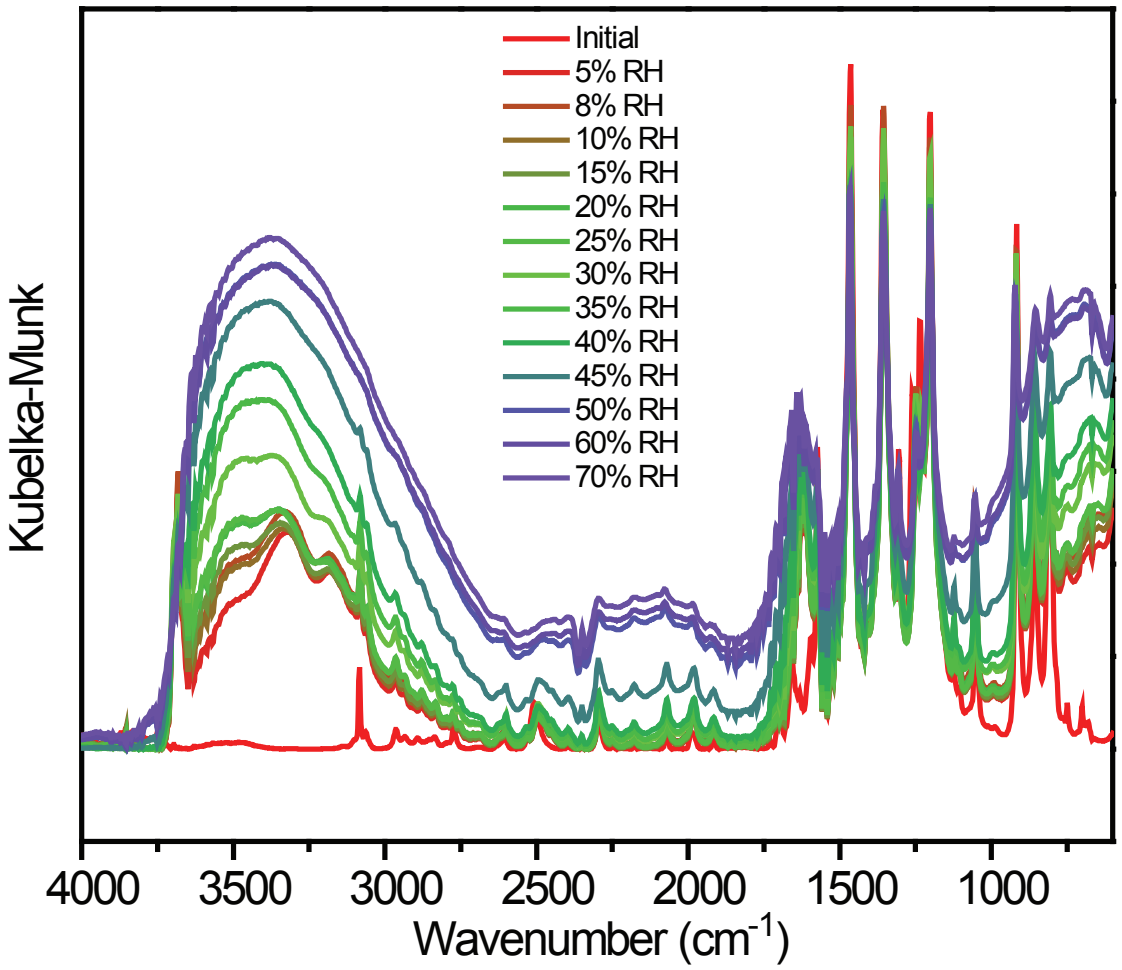

Figure S6.2. Diffuse-Reflectance Infrared Spectroscopy (DRIFTS) of the water adsorption process in Ni_2F_2BTDD under controlled relative humidity (RH).

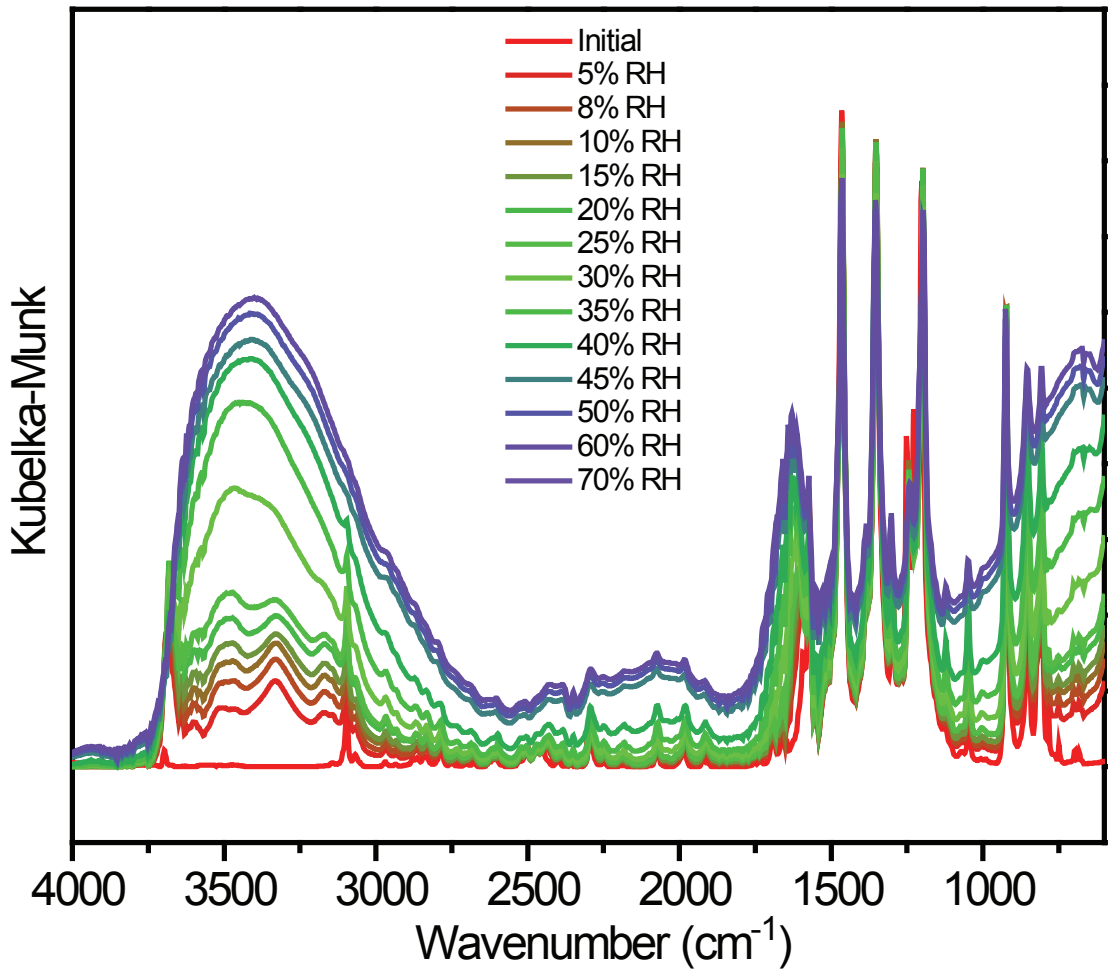

Figure S6.3. Diffuse-Reflectance Infrared Spectroscopy (DRIFTS) of the water adsorption process in Ni_2Cl_2BTDD under controlled relative humidity (RH).

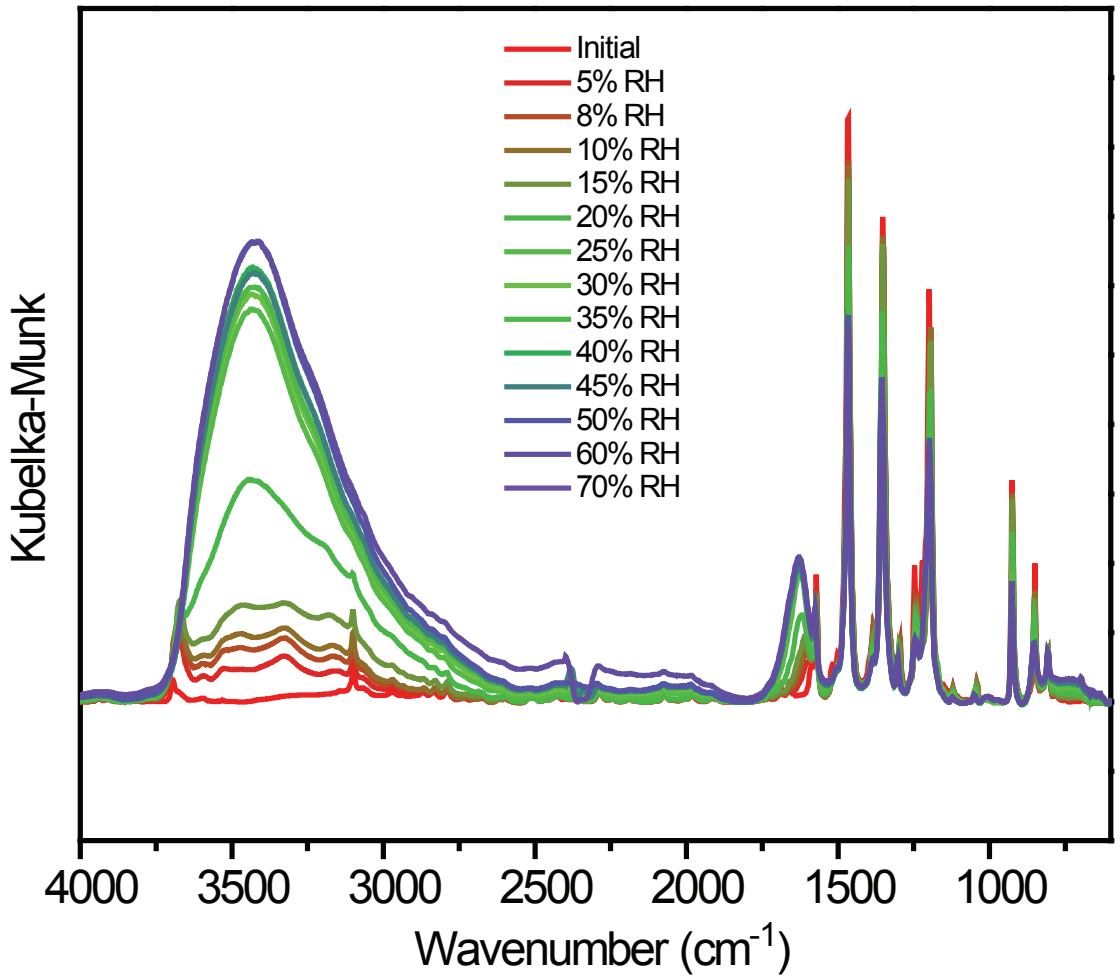

Figure S6.4. Diffuse-Reflectance Infrared Spectroscopy (DRIFTS) of the water adsorption process in Ni_2Br_2BTDD under controlled relative humidity (RH).

Section S7. Additional Water Cycling Data.

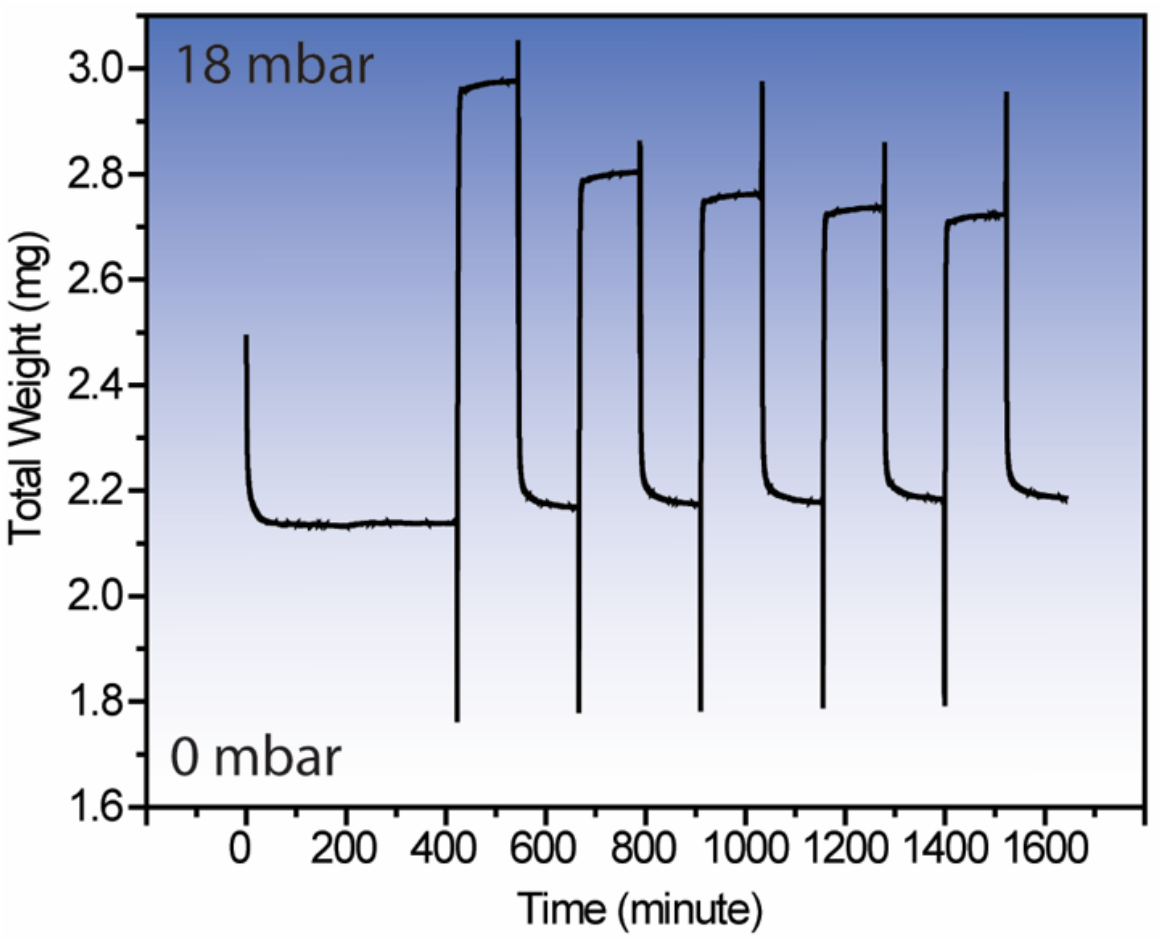

Figure S7.1: Water cycling in $Ni_2(OH)_2BTDD$, switching from 0 mbar H_2O to 18 mbar H_2O every two hours. Initial cycle was measured after a water isotherm at 25 °C. Spikes in data are microbalance anomalies caused by pressure changes.

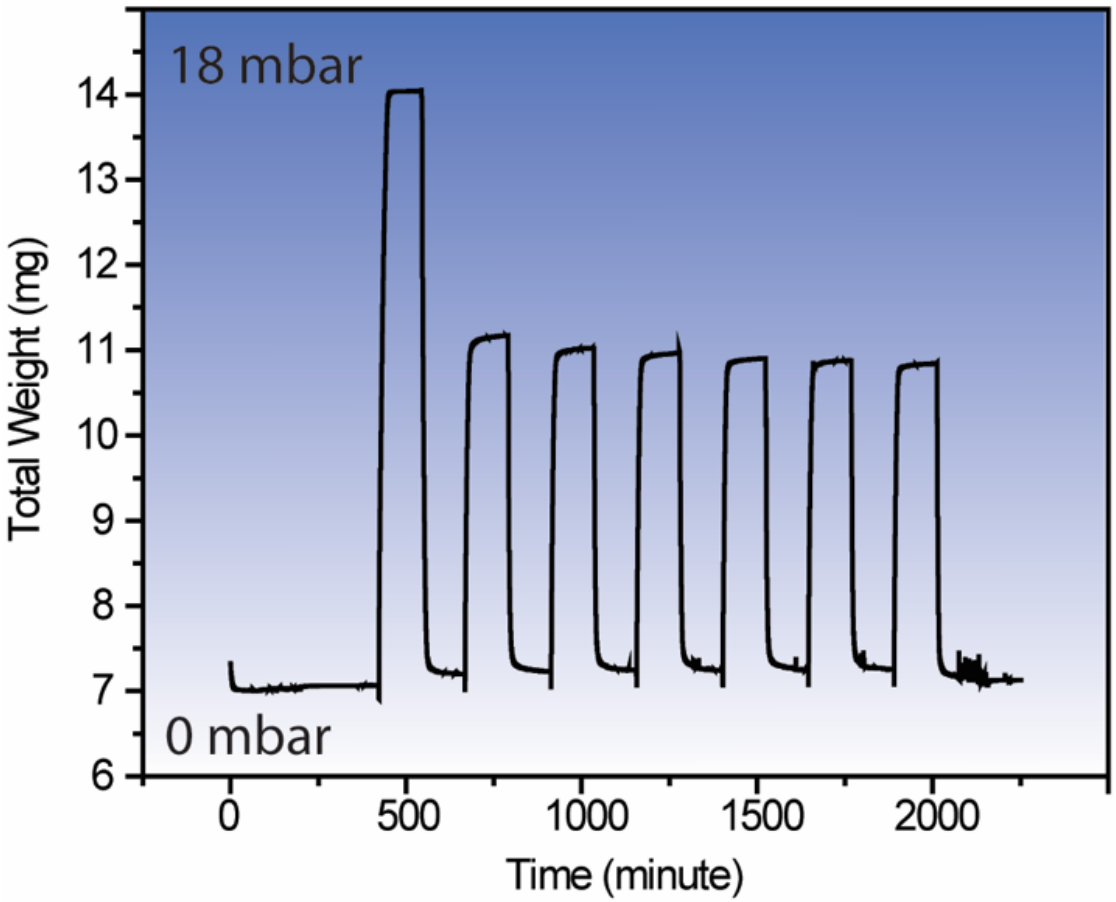

Figure S7.2: Water cycling in Ni_2F_2BTDD, switching from 0 mbar H_2O to 18 mbar H_2O every two hours. Initial cycle was measured after a water isotherm at 25 °C. Spikes in data are microbalance anomalies caused by pressure changes.

Section S8. Nuclear Magnetic Resonance Data.

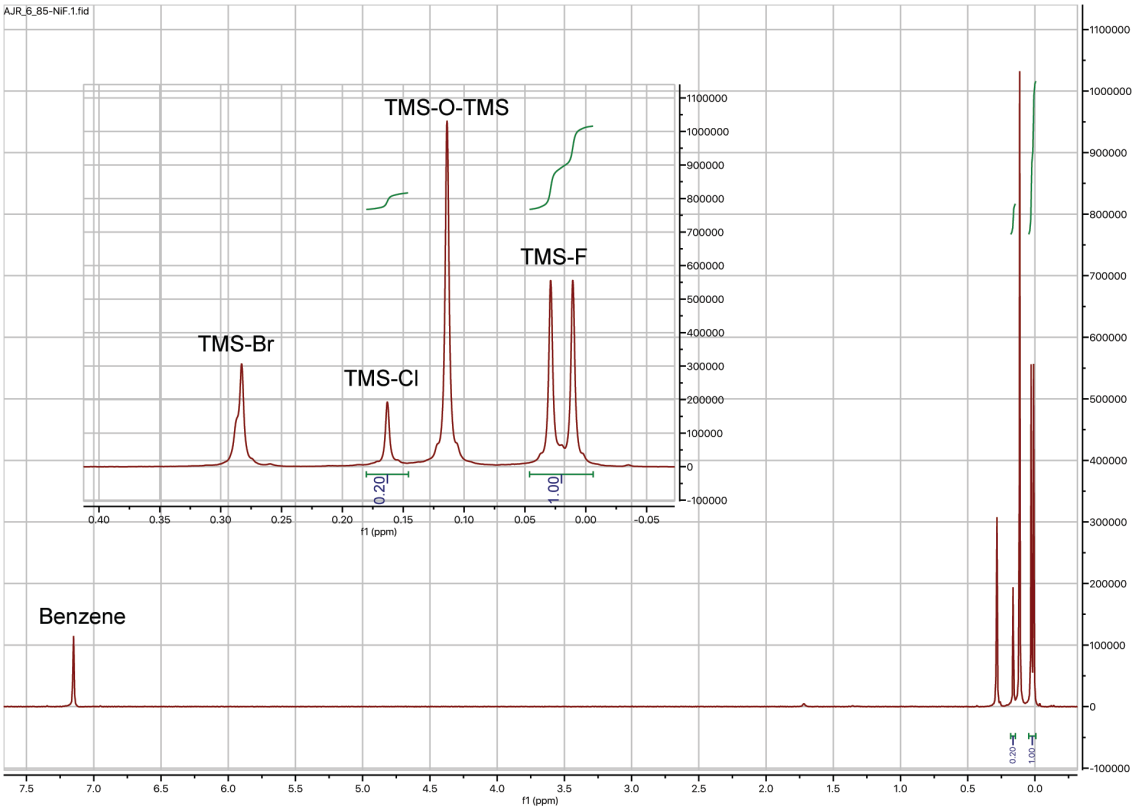

Figure S8.1: Nuclear Magnetic Resonance spectrum acquired at 400 MHz of the filtrate after treatment of Ni_2F_2BTDD with trimethylsilyl bromide (TMS-Br) in deuterated benzene.

Section S9. Rietveld Refinement of Synchrotron Powder X-ray Diffraction Data.

Due to relatively small crystal size, structures of **Ni_2X_2(BTDD)** were obtained from synchrotron powder X-ray diffraction data. Obtained patterns were refined in TOPAS Academic V6 (Coelho Software).[13] An anisotropic strain broadening model by Stephens et al. was used to improve profile fit.[14] Reported structures for **Co_2Cl_2(BTDD)**[11] and **Cu_2Cl_2(BTDD)**[15] were used as a starting point for the Rietveld refinement.[16] Structures were initially refined using a rigid body description of the ligand, with bond lengths and angles constrained to literature[15] values. After the orientation and position of the ligand were refined, the rigid body constraints were lifted, and all atom positions were refined, subject to geometric bond length and angle restraints. Distances and angles in the linker were restrained to literature values;[15] Ni-N1 and Ni-X distances were restrained to average Cambridge Structural Database[17] distances for the relevant Ni environments. Additional oxygen atoms representing adsorbed water molecules were placed in the MOF pores based on the difference Fourier map. For **Ni_2F_2(BTDD)**, the bridging halide was refined as a disorder between Cl and F to match the results of the NMR study. Initially, the occupancies of the halides were constrained to the experimental 1:5 ratio. The constraint was relaxed to a restraint in the final stage of the refinement. For **Ni_2Br_2(BTDD)**, the fit significantly improved with introduction of Ni and Br vacancies, and addition of a small amount of terminal Br (*Br2*) atoms disordered with the terminal water groups (*O2*) to keep the structure charge balanced. Thermal parameters were refined isotropically for all structures, with similarity restraints applied separately on heavy atoms and on light atoms. Experimental details and structural information are presented in Table **S9.1**. Final Rietveld plots for the three compounds are presented in Figs. **S9.1** (**Ni_2Cl_2(BTDD)**), **S9.2** (**Ni_2F_2(BTDD)**), and **S9.3** (**Ni_2Br_2(BTDD)**).

Table S9.1. Experimental details and structural information for Ni_2X_2(BTDD).

Material	**Ni_2F_2(BTDD)**	**Ni_2Cl_2(BTDD)**	**Ni_2Br_2(BTDD)**
Diffraction instrument	APS 11-BM		
Radiation type	Synchrotron X-ray		
Wavelength	0.412805 Å		
Temperature	100.0		
Formula	$C_{12}Cl_{0.38}F_{1.62}N_6Ni_2O_{8.56}$	$C_{12}Cl_2N_6Ni_2O_{11.48}$	$C_{12}Br_{1.63}N_6Ni_{1.81}O_{8.69}$
M_r, g mol^{-1}	526.79	600.19	603.91
Z	9		
Crystal system	Trigonal		
Space group	*$R\bar{3}m$ (no. 166; hexagonal setting)*		
a, Å	38.6092(5)	38.5282(5)	38.42498(19)
c, Å	8.09293(13)	8.18879(13)	8.20774(6)
V, Å^3	10447.6(3)	10527.1(3)	10494.98(13)
D_c, g cm^{-3}	0.75348	0.85204	0.85948
μ, mm^{-1}	0.196	0.215	0.496
2θ range, °	1 – 18	0.5 – 20	0.5 – 25
Refl. Obs.	628	846	1583
No. of parameters	65	65	71
No. of restraints	28	28	29
R_{wp}, %	7.08	7.71	7.83
R_{exp}, %	5.86	7.60	6.19
R_p, %	4.87	5.12	5.54
R_{Bragg}, %	0.91	1.38	1.92
GoF (χ)	1.21	1.01	1.27

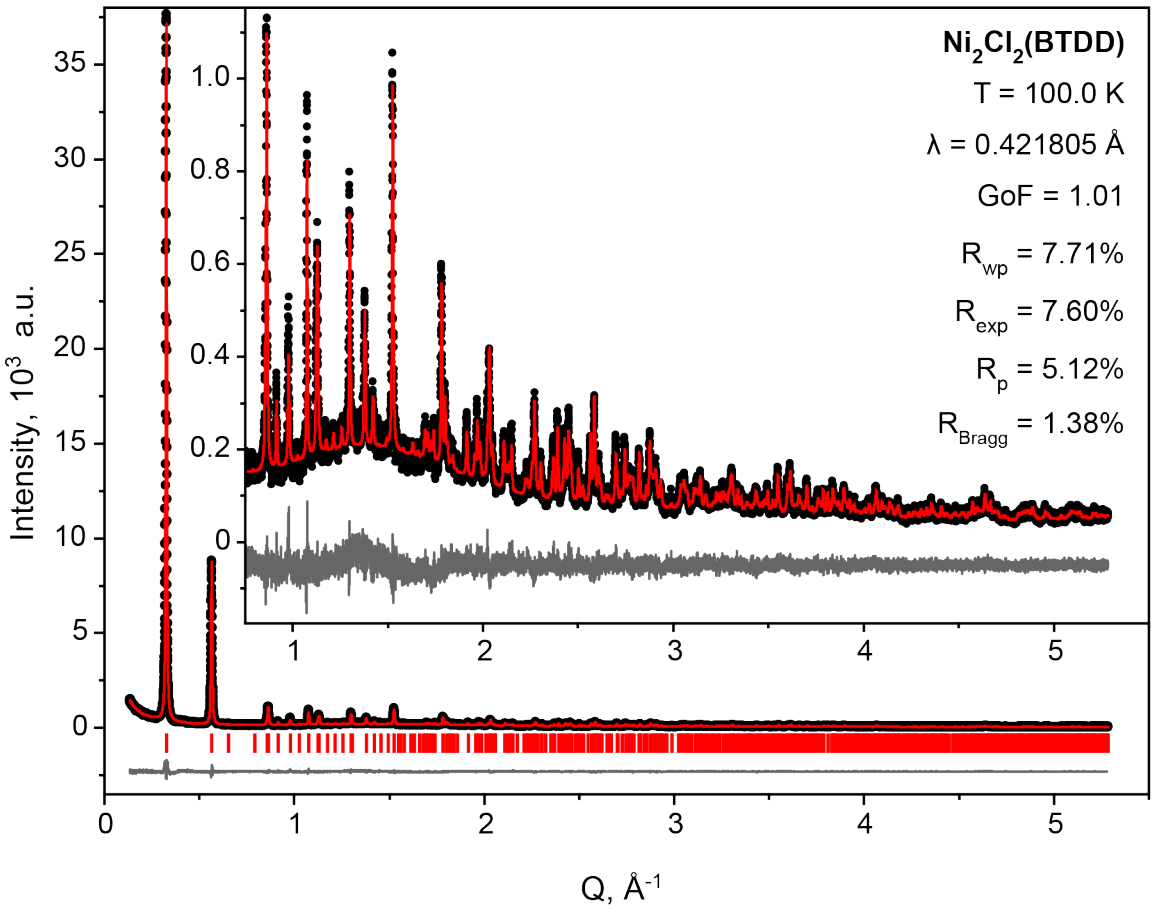

Figure S9.1. Rietveld fit of Ni_2Cl_2(BTDD). Red line: calculated intensities; black circles: experimental intensities; grey line: difference; red ticks: calculated reflection positions. Select fit parameters are presented on the plot.

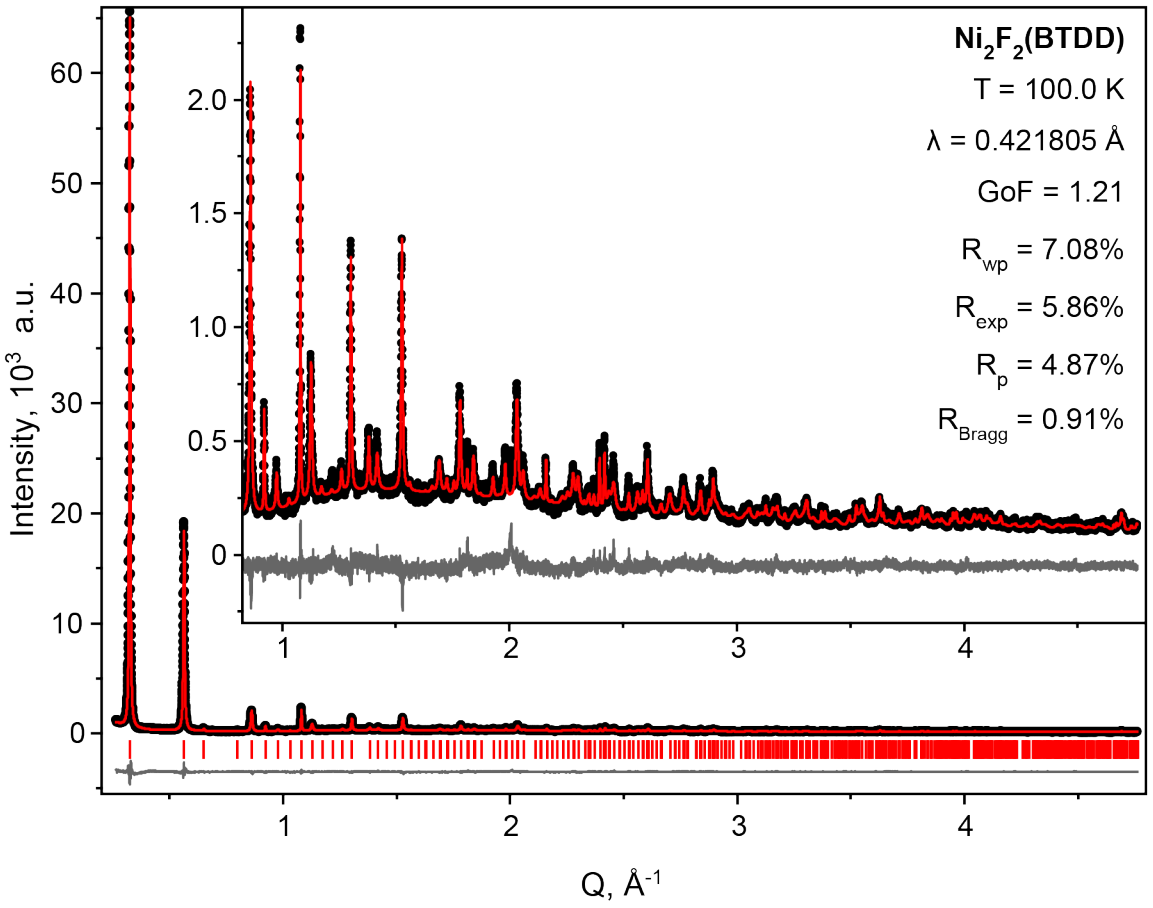

Figure S9.2. Rietveld fit of Ni_2F_2(BTDD). Red line: calculated intensities; black circles: experimental intensities; grey line: difference; red ticks: calculated reflection positions. Select fit parameters are presented on the plot.

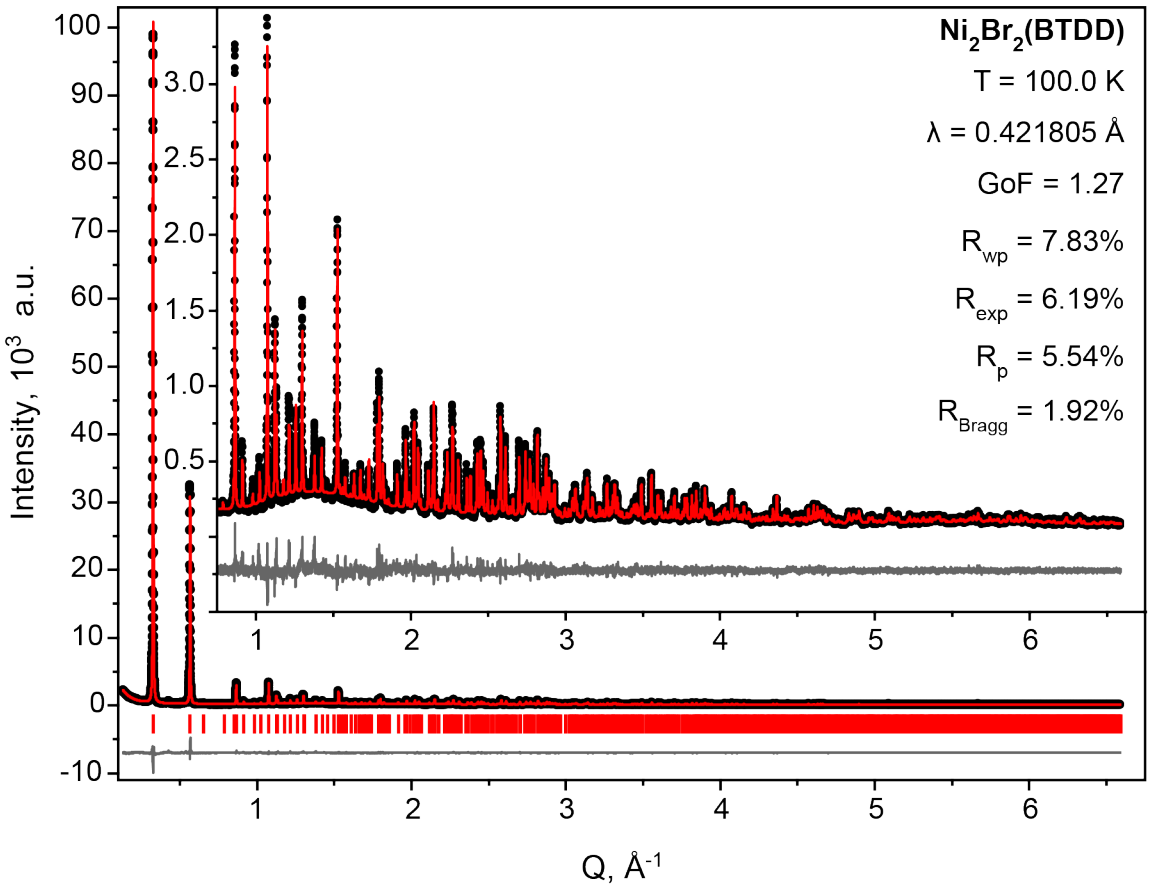

Figure S9.3. Rietveld fit of Ni_2Br_2(BTDD). Red line: calculated intensities; black circles: experimental intensities; grey line: difference; red ticks: calculated reflection positions. Select fit parameters are presented on the plot.

Section S10. Additional Water Uptake Data, Heat of Adsorption .

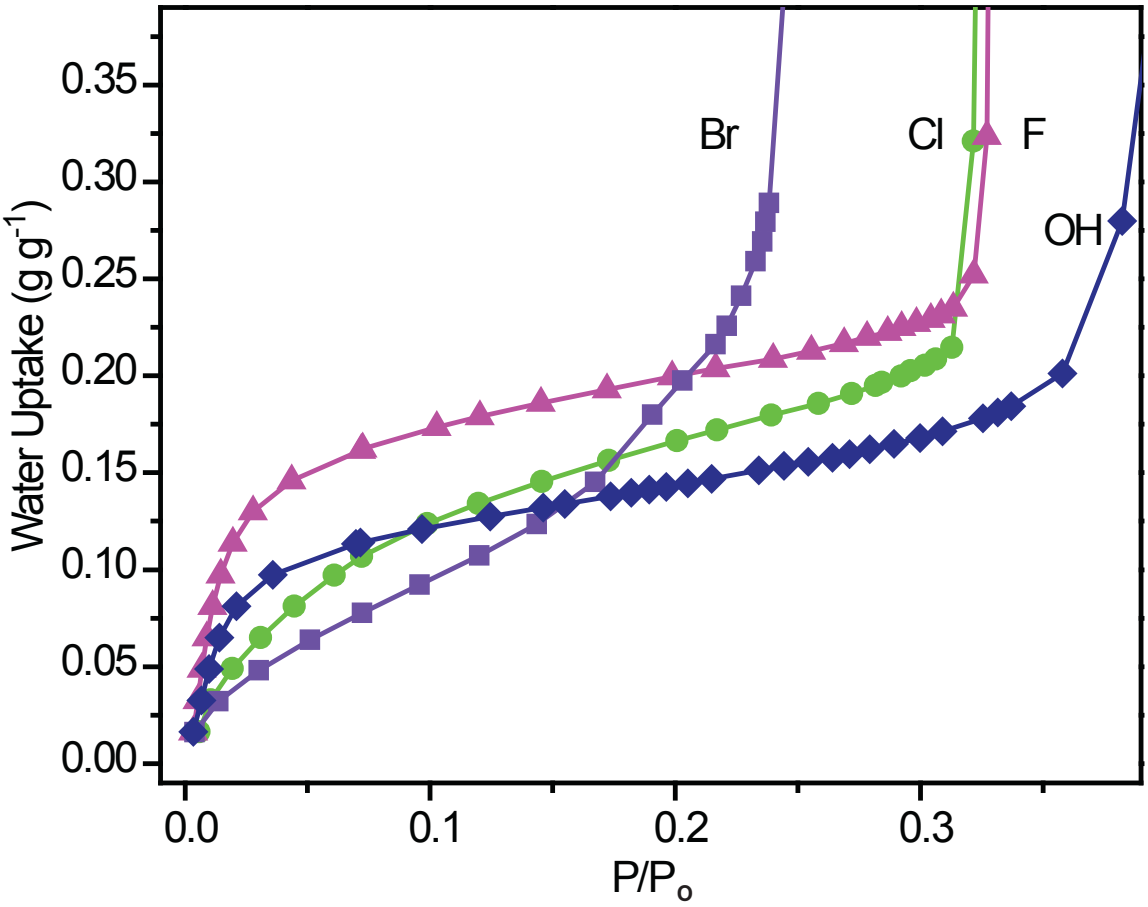

Figure S10.1: Zoom in on the low-pressure region of water adsorption isotherms in gravimetric units for Ni_2F_2BTDD (pink), Ni_2Cl_2BTDD (green), Ni_2Br_2BTDD (purple), and $Ni_2(OH)_2BTDD$ (navy).

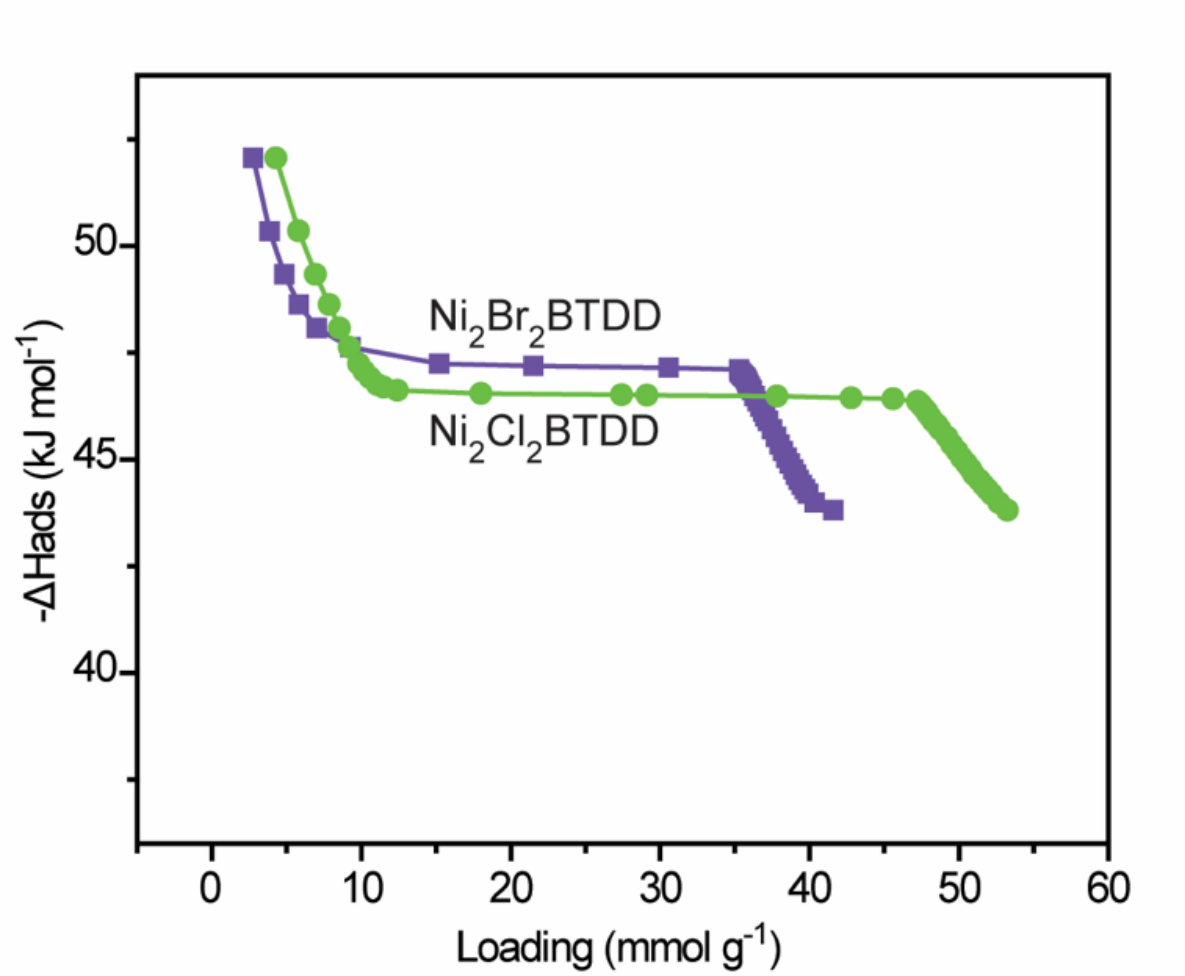

Figure S10.2: Heat of adsorption (ΔH_{ads}) of water in Ni_2Cl_2BTDD (green), or Ni_2Br_2BTDD (purple).

Section S11. References

(1) Kubelka, P.; Munk, F. Optics of Paint Layers. *Z Tech Phys* **1931**, *August*.

(2) Lee, P. L.; Shu, D.; Ramanathan, M.; Preissner, C.; Wang, J.; Beno, M. A.; Von Dreele, R. B.; Ribaud, L.; Kurtz, C.; Antao, S. M.; Jiao, X.; Toby, B. H. A Twelve-Analyzer Detector System for High-Resolution Powder Diffraction. *J. Synchrotron Radiat.* **2008**, *15* (5), 427–432.

(3) Wang, J.; Toby, B. H.; Lee, P. L.; Ribaud, L.; Antao, S. M.; Kurtz, C.; Ramanathan, M.; Von Dreele, R. B.; Beno, M. A. A Dedicated Powder Diffraction Beamline at the Advanced Photon Source: Commissioning and Early Operational Results. *Rev. Sci. Instrum.* **2008**, *79* (8), 085105.

(4) Shu, D.; Maser, J.; Holt, M.; Winarski, R.; Preissner, C.; Lai, B.; Vogt, S.; Stephenson, G. B. A Robot-Based Detector Manipulator System for a Hard X-Ray Nanoprobe Instrument. *Nucl. Instruments Methods Phys. Res. Sect. A Accel. Spectrometers, Detect. Assoc. Equip.* **2007**, *582* (1), 159–161.

(5) Perdew, J. P.; Ruzsinszky, A.; Csonka, G. I.; Vydrov, O. A.; Scuseria, G. E.; Constantin, L. A.; Zhou, X.; Burke, K. Restoring the Density-Gradient Expansion for Exchange in Solids and Surfaces. **2007**, *136406* (April), 1–4.

(6) Kresse, G.; Furthmüller, J. Efficient Iterative Schemes for Ab Initio Total-Energy Calculations Using a Plane-Wave Basis Set. *Phys. Rev. B - Condens. Matter Mater. Phys.* **1996**, *54* (16), 11169–11186.

(7) de Lange, M. F.; van Velzen, B. L.; Ottevanger, C. P.; Verouden, K. J. F. M.; Lin, L.-C.; Vlugt, T. J. H.; Gascon, J.; Kapteijn, F. Metal–Organic Frameworks in Adsorption-Driven Heat Pumps: The Potential of Alcohols as Working Fluids. *Langmuir* **2015**, *31* (46), 12783–12796.

(8) Cadiau, A.; Lee, J. S.; Damasceno Borges, D.; Fabry, P.; Devic, T.; Wharmby, M. T.; Martineau, C.; Foucher, D.; Taulelle, F.; Jun, C. H.; Hwang, Y. K.; Stock, N.; De Lange, M. F.; Kapteijn, F.; Gascon, J.; Maurin, G.; Chang, J. S.; Serre, C. Design of Hydrophilic Metal Organic Framework Water Adsorbents for Heat Reallocation. *Adv. Mater.* **2015**, *27* (32), 4775–4780.

(9) De Lange, M. F.; Verouden, K. J. F. M.; Vlugt, T. J. H.; Gascon, J.; Kapteijn, F. Adsorption-Driven Heat Pumps: The Potential of Metal-Organic Frameworks. *Chem. Rev.* **2015**, *115* (22), 12205–12250.

(10) Denysenko, D.; Grzywa, M.; Tonigold, M.; Streppel, B.; Krkljus, I.; Hirscher, M.; Mugnaioli, E.; Kolb, U.; Hanss, J.; Volkmer, D. Elucidating Gating Effects for Hydrogen Sorption in MFU-4-Type Triazolate-Based Metal-Organic Frameworks Featuring Different Pore Sizes. *Chem. - A Eur. J.* **2011**, *17* (6), 1837–1848.

(11) Rieth, A. J.; Tulchinsky, Y.; Dincă, M. High and Reversible Ammonia Uptake in Mesoporous Azolate Metal-Organic Frameworks with Open Mn, Co, and Ni Sites. *J. Am. Chem. Soc.* **2016**, *138* (30), 9401–9404.

(12) Wang, Y.; Huang, N. Y.; Shen, J. Q.; Liao, P. Q.; Chen, X. M.; Zhang, J. P. Hydroxide Ligands Cooperate with Catalytic Centers in Metal-Organic Frameworks for Efficient Photocatalytic CO2 Reduction. *J. Am. Chem. Soc.* **2018**, *140* (1), 38–41.

(13) Coelho, A. Topas Academic V6. *Coelho Softw.* **2017**.

(14) Stephens, P. W. Phenomenological Model of Anisotropic Peak Broadening in Powder Diffraction. *J. Appl. Crystallogr.* **1999**, *32* (2), 281–289.

(15) Park, S. S.; Tulchinsky, Y.; Dincă, M. Single-Ion Li^{+}, Na^{+}, and Mg^{2+} Solid Electrolytes

Supported by a Mesoporous Anionic Cu–Azolate Metal–Organic Framework. *J. Am. Chem. Soc.* **2017**, *139* (38), 13260–13263.
(16) Rietveld, H. M. A Profile Refinement Method for Nuclear and Magnetic Structures. *J. Appl. Crystallogr.* **1969**, *2* (2), 65–71.
(17) Groom, C. R.; Bruno, I. J.; Lightfoot, M. P.; Ward, S. C.; IUCr. The Cambridge Structural Database. *Acta Crystallogr. Sect. B Struct. Sci. Cryst. Eng. Mater.* **2016**, *72* (2), 171–179.